Three-flavor chiral phase structure in hot and dense QCD matter

B.-J. Schaefer[1,*] and M. Wagner[2,†]

[1]*Institut für Physik, Karl-Franzens-Universität, A-8010 Graz, Austria*
[2]*Institut für Kernphysik, TU Darmstadt, D-64289 Darmstadt, Germany*

Chiral symmetry restoration at nonzero temperature and quark densities are investigated in the framework of a linear sigma model with $N_f = 3$ light quark flavors. After the derivation of the grand potential in mean-field approximation, the nonstrange and strange condensates, the in-medium masses of the scalar and pseudoscalar nonets are analyzed in hot and dense medium. The influence of the axial anomaly on the nonet masses and the isoscalar mixings on the pseudoscalar η-η' and scalar $\sigma(600)$-$f_0(1370)$ complex are examined. The sensitivity of the chiral phase transition as well as the existence and location of a critical end point in the phase diagram on the value of the sigma mass are explored. The chiral critical surface with and without the influence of the axial $U(1)_A$ anomaly is elaborated as a function of the pion and kaon masses for several values of the sigma mass.

I. INTRODUCTION

The understanding of the properties of strongly interacting matter under extreme conditions is one of the most fascinating and challenging tasks. General features of hot and dense matter are summarized in the QCD phase diagram which can be probed by ultrarelativistic heavy ion experiments such as the RHIC (BNL), LHC (CERN) and the planned future CBM experiment at the FAIR facility in Darmstadt.

Theoretical considerations indicate that at high temperature and high baryon densities there should be a phase transition from ordinary hadronic matter to a chirally symmetric plasma of quarks and gluons [1]. Several issues concerning this transition are not yet clarified [2]. QCD in this temperature and density regime is a strongly coupled theory and hence perturbation theory cannot be used. In the absence of a systematically improvable and converging method to approach QCD at finite density one often turns to model investigations see, e.g., [3]. These models incorporate the important chiral symmetry breaking mechanism of QCD but neglect any effects of confinement. Only recently, certain aspects of confinement based on the Polyakov loop have been incorporated in chiral effective models in a systematic fashion [4,5] and interesting conclusions could be drawn (see, e.g., [6]).

The most prominent finding from low-energy chiral effective models is the QCD critical end point (CEP) [7]. Common to almost all effective model calculations is that the chiral phase transition is continuous in the low density region and discontinuous in the high density regime. Consequently, the endpoint where the phase transition ceases to be discontinuous is the QCD critical end point. Unfortunately, several obvious and related features such as

the exact location of this point in the QCD phase diagram cannot be predicted by these models.

On the other side, lattice QCD simulations are important alternatives to effective models' calculations and can gain much insights in the QCD phase structure [8–15]. Because of the notorious sign problem emerging at finite baryon density reliable predictions for QCD are still not conclusive. Even worse, recently different lattice methods that circumvent the sign problem are in conflict with each other. For example, using the imaginary chemical potential method for three physical quark masses no critical endpoint in the phase diagram is found [16–21].

The present work is an extension of a previous analysis within an effective linear sigma model (LσM) with two quark flavors to three quark flavors [22,23]. The restoration of the chiral $SU(3) \times SU(3)$ and axial $U(1)_A$ symmetries with temperature and quark chemical potentials is investigated. The axial $U(1)_A$ anomaly is considered via an effective 't Hooft determinant in the Lagrangian which breaks the $U(1)_A$ symmetry. The restoration of the $U(1)_A$ symmetry is linked to a vanishing of the topological susceptibility which can further be related to the η' mass via the Witten-Veneziano relation [24,25].

Some results depend sensitively on the model parameters which are tuned to reproduce the vacuum phenomenology. There are model-input parameters such as the σ meson mass which are poorly known experimentally. The generic findings of several parameter fits over a broad range of input parameters are compared. Furthermore, the extrapolation towards the chiral limit is also addressed and the mass sensitivity of the chiral phase structure is investigated.

The paper is organized as follows: after introducing the LσM with three quark flavors, some symmetry breaking patterns in the vacuum are briefly discussed. In Sec. III the grand thermodynamic potential is derived in mean-field approximation. In Sec. IV a discussion of the model pa-

*bernd-jochen.schaefer@uni-graz.at
†mathias.wagner@physik.tu-darmstadt.de

rameter fits is given. Since the experimental situation concerning the scalar σ-meson, $\sigma(600)$, is not settled we consider a wide range of different values of the σ-meson mass, m_σ, as input parameter. All parameter sets are collected in Appendix A.

For the LσM without quarks it is known that the standard loop expansion and related approximation methods at finite temperatures fail and imaginary meson masses are generated. In our approximation no such artifacts occur which enables us to perform a careful and detailed analysis of chiral symmetry restoration in hot and dense matter. This is demonstrated in Sec. V where the pseudoscalar and scalar meson masses at finite temperatures and chemical potentials with and without axial $U(1)_A$ symmetry breaking are investigated. All mass expressions are summarized in Appendix B. In addition, the scalar and pseudoscalar flavor mixing behavior in the medium is explored. Various definitions are deferred to Appendix C

The grand potential determines all thermodynamic properties. The resulting phase diagrams are presented in Sec. VI where the mass sensitivity of the chiral phase boundaries is also explored. Subsequently, the shape of the chiral critical surface which confines the region of the chiral first-order transitions in the m_π-m_K plane at the critical chemical potential is evaluated for several values of m_σ. Finally, in Sec. VII a summary with concluding remarks is given.

II. LINEAR SIGMA MODEL WITH THREE QUARK FLAVORS

The Lagrangian, $\mathcal{L}_{qm} = \mathcal{L}_q + \mathcal{L}_m$, of the $SU(3)_L \times SU(3)_R$ symmetric LσM with three quark flavors consists of the fermionic part

$$\mathcal{L}_q = \bar{q}(i\slashed{\partial} - gT_a(\sigma_a + i\gamma_5\pi_a))q \tag{1}$$

with a flavor-blind Yukawa coupling g of the quarks to the mesons and the purely mesonic contribution

$$\begin{aligned}\mathcal{L}_m &= \mathrm{Tr}(\partial_\mu\phi^\dagger\partial^\mu\phi) - m^2\,\mathrm{Tr}(\phi^\dagger\phi) - \lambda_1[\mathrm{Tr}(\phi^\dagger\phi)]^2 \\ &\quad - \lambda_2\,\mathrm{Tr}(\phi^\dagger\phi)^2 + c(\det(\phi) + \det(\phi^\dagger)) \\ &\quad + \mathrm{Tr}[H(\phi + \phi^\dagger)]. \end{aligned} \tag{2}$$

The column vector $q = (u, d, s)$ denotes the quark field for $N_f = 3$ flavors and $N_c = 3$ color degrees of freedom [26]. The ϕ-field represents a complex (3×3)-matrix and is defined in terms of the scalar σ_a and the pseudoscalar π_a meson nonet

$$\phi = T_a\phi_a = T_a(\sigma_a + i\pi_a). \tag{3}$$

The $T_a = \lambda_a/2$ with $a = 0, \ldots, 8$ are the nine generators of the $U(3)$ symmetry, where the λ_a are the usual eight Gell-Mann matrices and $\lambda_0 = \sqrt{\frac{2}{3}}\mathbf{1}$. The generators T_a are normalized to $\mathrm{Tr}(T_aT_b) = \delta_{ab}/2$ and obey the $U(3)$ algebra $[T_a, T_b] = if_{abc}T_c$ and $\{T_a, T_b\} = d_{abc}T_c$ respectively with the corresponding standard symmetric d_{abc} and antisymmetric f_{abc} structure constants of the $SU(3)$ group and

$$f_{ab0} = 0, \qquad d_{ab0} = \sqrt{\frac{2}{3}}\delta_{ab}. \tag{4}$$

Chiral symmetry is broken explicitly by the last term in Eq. (2) where

$$H = T_ah_a \tag{5}$$

is a (3×3)-matrix with nine external parameters h_a. In general, one could add further explicit symmetry breaking terms to $\mathcal{L}_m$ which are nonlinear in ϕ [27,28], but this is ignored in this work.

Because of spontaneous chiral symmetry breaking in the vacuum a finite vacuum expectation value of the ϕ field, $\bar{\phi}$, is generated which must carry the quantum numbers of the vacuum [29]. As a consequence, only the diagonal components h_0, h_3 and h_8 of the explicit symmetry breaking term can be nonzero. This in turn involves three finite condensates $\bar{\sigma}_0$, $\bar{\sigma}_3$ and $\bar{\sigma}_8$ of which $\bar{\sigma}_3$ breaks the $SU(2)$ isospin symmetry. In the following we shall restrict ourselves to a $2 + 1$ flavor symmetry breaking pattern and neglect the violation of the isospin symmetry. This is reflected by the choice $h_0 \neq 0$, $h_3 = 0$, $h_8 \neq 0$ and corresponds to two degenerated light quark flavors (u, d) and one heavier quark flavor (s).

Besides the explicit symmetry breaking terms h_0 and h_8 the model has five more parameters: the squared tree-level mass of the meson fields m^2, two possible quartic coupling constants λ_1 and λ_2, a Yukawa coupling g and a cubic coupling constant c which models the axial $U(1)_A$ anomaly of the QCD vacuum. The $U(1)_A$ symmetry of the classical QCD Lagrangian is anomalous [30], i.e., broken by quantum effects. Without the anomaly a ninth pseudoscalar Goldstone boson corresponding to the spontaneous breaking of the chiral $U(3)_L \times U(3)_R$ symmetry should emerge. However, experimentally, the lightest candidate for this boson is the η' meson, whose mass is of the order $m_{\eta'} \sim 960$ MeV which is far from being a light Goldstone boson. The explicit breaking of the $U(1)_A$ symmetry is held responsible for the fact that the η' mass is considerably larger than all other pseudoscalar meson masses. This well-known $U(1)_A$ problem of QCD is effectively controlled by the anomaly term c in the Lagrangian. The comprehensive procedure of how to fix the parameters will be given in Sec. IV.

Depending on the signs and values of the parameters several possible symmetry breaking patterns in the vacuum can be obtained (see also [28] for more details). Without explicit symmetry breaking terms, i.e. for $H = 0$, and without an explicit $U(1)_A$ symmetry breaking term, i.e.

for $c = 0$, the Lagrangian has a global $SU(3)_V \times U(3)_A \simeq SU(3)_V \times SU(3)_A \times U(1)_A$ symmetry if the quartic coupling λ_2 and m^2 are positive.[1] If the mass parameter m^2 changes sign the symmetry is spontaneously broken down to $SU(3)_V$. The first quartic coupling λ_1 has no influence on the symmetry breaking. Because of the breaking of the $U(3)_A$ symmetry nine pseudoscalar Goldstone bosons arise which form the entire nonet consisting of three pions, four kaons, the η and η' meson. The scalar nonet belongs to the $SU(3)_V$ group which has a singlet and an octet representation. All masses of the octet particles are degenerate. The σ meson belongs to the singlet and its mass is in general different from the masses of the other octet particles.

By setting $c \neq 0$ the effects of the $U(1)_A$ symmetry breaking, caused by a nonvanishing topological susceptibility, are included and the symmetry of the Lagrangian is reduced to $SU(3)_V \times SU(3)_A$. Because of the spontaneous symmetry breaking of the $SU(3)_A$, the vacuum has a $SU(3)_V$ symmetry. In this case the entire pseudoscalar octet is degenerated and only eight Goldstone bosons appear. The η' meson, the would-be Goldstone boson, is still massive in this case. The masses of the scalar particles are not modified by the $U(1)_A$ breaking.

With explicit symmetry breaking terms, more precisely, for only finite h_0 and h_8 terms, the vacuum $SU(3)_V$ symmetry is explicitly broken down to the isospin $SU(2)_V$ symmetry since the h_3 term is set to zero. This symmetry pattern is already a good approximation to nature because the violation of the isospin symmetry is small anyway. The resulting ground state spectrum for this symmetry pattern will be discussed in Sec. V B.

III. GRAND POTENTIAL

In this section, the derivation of the grand thermodynamic potential for the three-flavor model is given. We will use a mean-field approximation similar to the one for the two-flavor model in [22]. The mean-field approximation is simple in its application, in particular, at finite temperature and quark densities. Low-energy theorems, such as, e.g., the Goldstone theorem or the Ward identities are also fulfilled at finite temperatures and densities. In this way we can circumvent more advanced many-body resummation techniques which are usually necessary to cure the breakdown of naive perturbation theory due to infrared divergences. For example, it is well-known that the standard loop expansion or related expansion methods of the $SU(3)$ version of the LσM with or without quarks break down at finite temperature and imaginary meson masses are generated in the spontaneously broken phase [31–35].

Contributions of thermal excitations to the meson masses are neglected in these approximation schemes which result in a too rapid decrease of the meson masses, and, e.g., the squared pion mass becomes negative for temperatures much below the phase transition. This deficiency can be cured by self-consistent resummation schemes such as the Hartree approximation in the Cornwall-Jackiw-Tomboulis formalism [34,36] or the so-called Optimized Perturbation Theory (OPT) e.g., [37] and variants thereof. Recently, the OPT method has been frequently applied to the three-flavor LσM with and without quarks at finite temperature and baryon densities [38,39]. However, the predictive power of the OPT method depends on how it is implemented and approximations thereof are made. For instance, when the external momentum of the self-energy are taken on-shell a solution of the corresponding gap equation and also of the equation of state cease to exist above a certain temperature, particularly below the critical one. Details and some improvements of certain approximations in the OPT framework can be found in [38,39].

All these problems do not emerge in the mean-field approximation used here. This enables us to study the phase structure of the more involved three-flavor model in great detail and in a rather simple framework.

In order to calculate the grand potential in mean-field approximation we start from the partition function. In thermal equilibrium, the grand partition function is defined by a path integral over the quark/antiquark and meson fields

$$Z = \int \prod_a \mathcal{D}\sigma_a \mathcal{D}\pi_a \int \mathcal{D}q \mathcal{D}\bar{q}$$
$$\times \exp\left(-\int_0^{1/T} d\tau \int_V d^3x \mathcal{L}^E\right), \qquad (6)$$

where T is the temperature and V the three-dimensional volume of the system.[2] For three quark flavors the Euclidean Lagrangian $\mathcal{L}^E$ generally contains three independent quark chemical potentials μ_f

$$\mathcal{L}^E = \mathcal{L}_{qm} + \sum_{f=u,d,s} \mu_f q_f^\dagger q_f.$$

Because of the assumed $SU(2)_V$ isospin symmetry we neglect the slight mass difference between an u- and d-quark and the light quark chemical potentials become equal. In the following we denote the degenerated light quark quantities by an index q, i.e., the light quark chemical potential by $\mu_q \equiv \mu_u = \mu_d$, and the strange quark quantities by an index s.

The calculation of the partition function in the mean-field approximation is performed similar to Refs. [22,40] for the two-flavor case. The quantum and thermal fluctuations of the mesons are neglected and the quarks/antiquarks

---

[1]More precisely, without the determinant the Lagrangian $\mathcal{L}_{qm}$ is $U(3) \times U(3)$ invariant which is isomorphic to $SU(3)_L \times SU(3)_R \times U(1)_B \times U(1)_A$. The $U(1)_B$ is related to the baryon number and is always conserved which is why we have neglected it.

[2]An irrelevant normalization constant is suppressed.

are retained as quantum fields. This means that the integration over the mesonic fields in Eq. (6) is dropped and the fields are replaced by their nonvanishing vacuum expectation values $\bar{\phi} = T_0 \bar{\sigma}_0 + T_8 \bar{\sigma}_8$. The remaining integration over the Grassmann fields yields a determinant which can be rewritten as a trace over a logarithm. Evaluating the trace within the Matsubara formalism, the quark contribution $\Omega_{\bar{q}q}(T, \mu_f)$ of the grand potential is obtained [41]. The ultraviolet divergent vacuum contribution to $\Omega_{\bar{q}q}(T, \mu_f)$ which results from the negative energy states of the Dirac sea has been neglected here (cf. [22,40] for further details). Finally, the total grand potential is obtained as a sum of the quark contribution and meson contribution $U(\bar{\sigma}_0, \bar{\sigma}_8)$ as

$$\Omega(T, \mu_f) = \frac{-T \ln \mathcal{Z}}{V} = U(\bar{\sigma}_0, \bar{\sigma}_8) + \Omega_{\bar{q}q}(T, \mu_f). \quad (7)$$

Explicitly, the quark contribution reads

$$\Omega_{\bar{q}q}(T, \mu_f) = \nu_c T \sum_{f=u,d,s} \int_0^\infty \frac{d^3k}{(2\pi)^3} \{\ln(1 - n_{q,f}(T, \mu_f)) + \ln(1 - n_{\bar{q},f}(T, \mu_f))\} \quad (8)$$

with the usual fermionic occupation numbers for the quarks

$$n_{q,f}(T, \mu_f) = \frac{1}{1 + \exp((E_{q,f} - \mu_f)/T)} \quad (9)$$

and antiquarks $n_{\bar{q},f}(T, \mu_f) \equiv n_{q,f}(T, -\mu_f)$ respectively. The number of internal quark degrees of freedom is denoted by $\nu_c = 2N_c = 6$. The flavor-dependent single-particle energies are

$$E_{q,f} = \sqrt{k^2 + m_f^2} \quad (10)$$

with the flavor-dependent quark masses m_f which are also functions of the expectation values $\bar{\sigma}_0$ and $\bar{\sigma}_8$.

The vacuum condensates $\bar{\sigma}_0$ and $\bar{\sigma}_8$ are members of the scalar ($J^P = 0^+$) nonet and both contain strange and nonstrange components. For further analysis it is more convenient to convert the condensates into a pure nonstrange and strange part. This is achieved by an orthogonal basis transformation from the original octet-singlet basis (σ_0, σ_8) to the nonstrange (σ_x) and strange (σ_y) quark flavor basis

$$\begin{pmatrix} \sigma_x \\ \sigma_y \end{pmatrix} = \frac{1}{\sqrt{3}} \begin{pmatrix} \sqrt{2} & 1 \\ 1 & -\sqrt{2} \end{pmatrix} \begin{pmatrix} \sigma_0 \\ \sigma_8 \end{pmatrix}. \quad (11)$$

As a consequence, the light quark sector decouples from the strange quark sector (cf., e.g., [39]) and the quark masses simplify in this new basis to

$$m_q = g\sigma_x/2, \qquad m_s = g\sigma_y/\sqrt{2}. \quad (12)$$

The meson potential modifies accordingly

$$
\begin{aligned}
U(\sigma_x, \sigma_y) = & \frac{m^2}{2}(\sigma_x^2 + \sigma_y^2) - h_x \sigma_x - h_y \sigma_y - \frac{c}{2\sqrt{2}} \sigma_x^2 \sigma_y \\
& + \frac{\lambda_1}{2} \sigma_x^2 \sigma_y^2 + \frac{1}{8}(2\lambda_1 + \lambda_2)\sigma_x^4 \\
& + \frac{1}{8}(2\lambda_1 + 2\lambda_2)\sigma_y^4,
\end{aligned} \quad (13)
$$

therein the explicit symmetry breaking parameters h_0 and h_8 have also been transformed according to Eq. (11). The order parameters for the chiral phase transition are identified here with the expectation value $\bar{\sigma}_x$ for the nonstrange and with $\bar{\sigma}_y$ for the strange sector. They are obtained by minimizing the total thermodynamic potential (7) in the nonstrange and strange directions

$$\frac{\partial \Omega}{\partial \sigma_x} = \frac{\partial \Omega}{\partial \sigma_y}\bigg|_{\sigma_x = \bar{\sigma}_x, \sigma_y = \bar{\sigma}_y} = 0. \quad (14)$$

The solutions of these coupled equations determine the behavior of the chiral order parameters as a function of T and chemical potentials, μ_q and μ_s. Note that the in-medium condensates are also labeled with a bar over the corresponding fields.

IV. PARAMETER FITS

The LσM with three quark flavors has altogether seven parameters m^2, λ_1, λ_2, c, g, h_0, h_8 and two unknown condensates $\bar{\sigma}_x$ and $\bar{\sigma}_y$. The six parameters m^2, λ_1, λ_2, c, h_x and h_y of the mesonic potential are fixed in the vacuum by six experimentally known quantities. Similar to Ref. [34], we have chosen as input the low-lying pseudo-scalar mass spectrum, m_π and m_K, the average squared mass of the η and η' mesons, $m_\eta^2 + m_{\eta'}^2$, and the decay constants of the pion and kaon, f_π and f_K, and in addition the scalar σ meson mass m_σ. We can then predict the scalar meson masses m_{a_0}, m_κ, m_{f_0}, the difference of the η, η' squared masses, $m_\eta^2 - m_{\eta'}^2$ and the scalar and pseudoscalar mixing angles θ_S, θ_P.

In analogy to, e.g., Ref. [34] the values of the condensates are determined from the pion and kaon decay constants by means of the partially conserved axial-vector current relation (PCAC). In the strange-non-strange basis they are given by

$$\bar{\sigma}_x = f_\pi, \qquad \bar{\sigma}_y = \frac{1}{\sqrt{2}}(2f_K - f_\pi). \quad (15)$$

The average squared η and η' meson mass determines the parameter λ_2 by

$$\lambda_2 = \frac{3(2f_K - f_\pi)m_K^2 - (2f_K + f_\pi)m_\pi^2 - 2(m_{\eta'}^2 + m_\eta^2)(f_K - f_\pi)}{(3f_\pi^2 + 8f_K(f_K - f_\pi))(f_K - f_\pi)}, \tag{16}$$

and the $U(1)_A$ anomaly breaking term c is fixed by λ_2 and the difference of the pion and kaon masses squared via

$$c = \frac{m_K^2 - m_\pi^2}{f_K - f_\pi} - \lambda_2(2f_K - f_\pi). \tag{17}$$

Note, that without anomaly breaking, i.e. for $c = 0$, the average η-η' meson mass is not used anymore for fixing the parameter λ_2. It is then given by the kaon and pion masses and decay constants only,

$$\lambda_2 = \frac{m_K^2 - m_\pi^2}{(2f_K - f_\pi)}(f_K - f_\pi). \tag{18}$$

The input parameters from the pseudoscalar sector involve only a relation between λ_1 and m^2. Therefore, further input from the scalar sector is necessary. In principle two possible options are available. At first, the parameter m^2 is expressed as a function of the yet undetermined parameter λ_1. This can be achieved by using the equation for the pion mass or the kaon mass (see Appendix B). In this way the m^2 dependence of the σ meson mass (or of the $f_0(1370)$ meson mass) can be transformed in a λ_1 dependence since the scalar mixing angle does not depend on m^2. By fixing the mass of the σ meson (or of the $f_0(1370)$ meson) λ_1 is determined by solving the corresponding equation. Afterwards, the m^2 parameter follows immediately, since λ_1 is fixed.

The explicit symmetry breaking terms h_x and h_y in the non-strange-strange basis are related to the pion and kaon masses by the Ward identities

$$h_x = f_\pi m_\pi^2, \qquad h_y = \sqrt{2}f_K m_K^2 - \frac{f_\pi m_\pi^2}{\sqrt{2}}. \tag{19}$$

These relations can be derived by using the gap equations, Eqs. (14). The last open parameter, the value of the Yukawa coupling g, is fixed from the nonstrange constituent quark mass

$$g = 2m_q/\bar{\sigma}_x. \tag{20}$$

For example, using for the light constituent quark mass a value of $m_q = 300$ MeV we obtain $g \sim 6.5$ and can predict a strange constituent quark mass $m_s \approx 433$ MeV.

Since the experimental situation concerning the broad σ (or $f_0(600)$) resonance is not yet clear, cf. [42], we will use different input values for m_σ in the range of $m_\sigma = 400$–1000 MeV and will investigate its mass dependence on various quantities (see also [43]). In Appendix A several parameter sets for different m_σ values with and without effects of the axial $U(1)_A$ anomaly are summarized (Table I). Furthermore, a discussion of the parameter sets with respect to spontaneous symmetry breaking can be found in this appendix. The corresponding predictions of the scalar and pseudoscalar meson masses and mixing angles are collected in Table II

V. CHIRAL SYMMETRY RESTORATION

Having fixed the model parameters we can now evaluate the grand potential numerically. In the following we present our results for the chiral symmetry restoration at finite temperature and finite quark density with and without axial anomaly breaking. Throughout this section, the axial anomaly breaking term is kept constant, in particular, independent of the temperature and the chemical potentials.

TABLE I.   Different parameter sets for various m_σ with ($c \neq 0$) and without ($c = 0$) $U(1)_A$ anomaly.

m_σ [MeV]	c [MeV]	λ_1	m^2 [MeV^2]	λ_2	h_x [MeV^3]	h_y [MeV^3]
400	0	-24.55	$+(309.41)^2$	82.47	$(120.73)^3$	$(336.41)^3$
500	0	-21.24	$+(194.82)^2$	82.47	$(120.73)^3$	$(336.41)^3$
600	0	-17.01	$-(189.85)^2$	82.47	$(120.73)^3$	$(336.41)^3$
700	0	-11.61	$-(360.91)2$	82.47	$(120.73)^3$	$(336.41)^3$
800	0	-4.55	$-(503.55)^2$	82.47	$(120.73)^3$	$(336.41)^3$
900	0	5.56	$-(655.82)^2$	82.47	$(120.73)^3$	$(336.41)^3$
1000	0	24.22	$-(869.50)^2$	82.47	$(120.73)^3$	$(336.41)^3$
400	4807.84	-5.90	$+(494.75)^2$	46.48	$(120.73)^3$	$(336.41)^3$
500	4807.84	-2.70	$+(434.56)^2$	46.48	$(120.73)^3$	$(336.41)^3$
600	4807.84	1.40	$+(342.52)^2$	46.48	$(120.73)^3$	$(336.41)^3$
700	4807.84	6.62	$+(161.98)^2$	46.48	$(120.73)^3$	$(336.41)^3$
800	4807.84	13.49	$-(306.26)^2$	46.48	$(120.73)^3$	$(336.41)^3$
900	4807.84	23.65	$-(520.80)^2$	46.48	$(120.73)^3$	$(336.41)^3$
1000	4807.84	45.43	$-(807.16)^2$	46.48	$(120.73)^3$	$(336.41)^3$

TABLE II. Meson masses and mixing angles in the vacuum for different sets of parameters. The first five columns are input while the remaining columns are predictions. Upper block: without ($c = 0$) $U(1)_A$ anomaly, lower block: with $U(1)_A$ anomaly. Last line: experimental values from the PDG [42].

m_σ	m_π	m_K	$m_{\eta'}$	m_η	θ_P	m_{a_0}	m_κ	m_{f_0}	θ_S
400	138	496	138.0	634.8	35.3	850.4	1124.3	1257.3	16.7
500	138	496	138.0	634.8	35.3	850.4	1124.3	1267.4	18.7
600	138	496	138.0	634.8	35.3	850.4	1124.3	1282.3	21.5
700	138	496	138.0	634.8	35.3	850.4	1124.3	1304.9	25.5
800	138	496	138.0	634.8	35.3	850.4	1124.3	1341.4	31.3
900	138	496	138.0	634.8	35.3	850.4	1124.3	1408.0	40.0
1000	138	496	138.0	634.8	35.3	850.4	1124.3	1563.4	53.2
400	138	496	963.0	539.0	−5.0	1028.7	1124.3	1198.4	14.9
500	138	496	963.0	539.0	−5.0	1028.7	1124.3	1207.5	16.9
600	138	496	963.0	539.0	−5.0	1028.7	1124.3	1221.1	19.9
700	138	496	963.0	539.0	−5.0	1028.7	1124.3	1242.3	24.2
800	138	496	963.0	539.0	−5.0	1028.7	1124.3	1278.0	30.7
900	138	496	963.0	539.0	−5.0	1028.7	1124.3	1348.0	40.9
1000	138	496	963.0	539.0	−5.0	1028.7	1124.3	1545.6	57.1
400–1200	138.0	496	957.78	547.5		984.7	1414	1200–1500	

A. Condensates

The chiral phase structure of the underlying three-flavor model is completely governed by the total thermodynamic potential. Hence, the solution of the gap Eqs. (14) determines the behavior of the condensates as a function of temperature and quark chemical potentials. In general, the three quark chemical potentials are independent but here we will consider symmetric quark matter and define a uniform chemical potential $\mu \equiv \mu_q = \mu_s$.

In Fig. 1 the nonstrange $\bar\sigma_x$ and strange $\bar\sigma_y$ condensates are shown as a function of temperature for vanishing chemical potential μ for $m_\sigma = 800$ MeV. The reason for choosing this value for m_σ will become clear later on, see also Appendix A. The solid lines in this figure are obtained
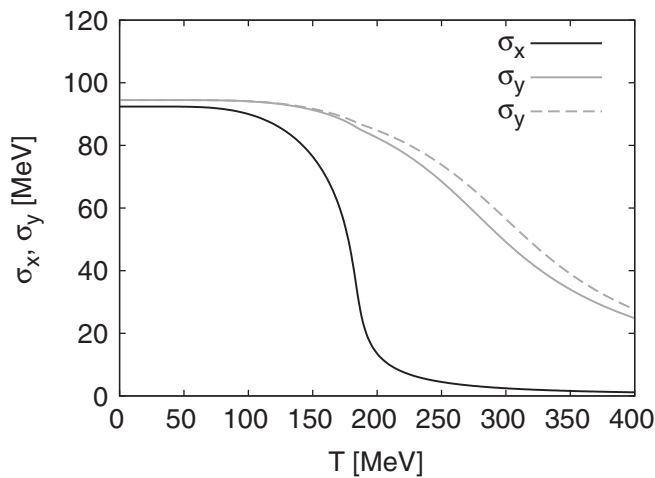

FIG. 1. The nonstrange, $\bar\sigma_x$ and strange, $\bar\sigma_y$ condensates as a function of temperature for vanishing chemical potentials with (solid) and without $U(1)_A$ anomaly (dashed). The anomaly does not modify the nonstrange condensate.

with an explicit axial $U(1)_A$ symmetry breaking term while the dashed line corresponds to the anomaly-free case, i.e. $c = 0$. The difference in the nonstrange condensate $\bar\sigma_x$, caused by the anomaly, is not visible in the figure. The condensates start at $T = 0$ with the fitted values, $\bar\sigma_x = 92.4$ MeV and $\bar\sigma_y = 94.5$ MeV. The temperature behavior of both condensates shows a smooth crossover. The temperature derivative of the nonstrange condensate peaks around $T \sim 181$ MeV. The precise value of this pseudocritical temperature depends on the value of m_σ in the vacuum. For smaller values of m_σ the pseudocritical temperature decreases (cf. Sec. VI). The chiral transition in the strange sector is much smoother due to the larger constituent strange quark mass, $m_s = 433$ MeV. As a consequence, the chiral $SU(2) \times SU(2)$ symmetry is restored more rapidly. With axial anomaly the strange condensate melts a little earlier but only for temperatures above the transition. At very high temperatures both condensates become degenerate, indicating chiral $SU(3) \times SU(3)$ symmetry restoration.

If one uses a temperature-dependent anomaly term by making use of lattice results for the topological susceptibility which yields, e.g., a decreasing anomaly term for increasing temperatures, a faster effective restoration of the axial symmetry can be achieved, see, e.g., [44,45].

For zero temperature and finite chemical potential both condensates are independent of μ in the broken phase until the Fermi surface of the light quarks is reached. For zero temperature the light Fermi surface coincides with the light quark mass, i.e. $\mu = m_q = 300$ MeV. Before the chiral transition takes place at a critical chemical potential $\mu_c \sim 352$ MeV the nonstrange condensate drops by about 10% from its vacuum value as can be seen in Fig. 2. At μ_c the phase transition is of first-order and three solutions of each gap Eq. (14) appear corresponding to two degenerate min-
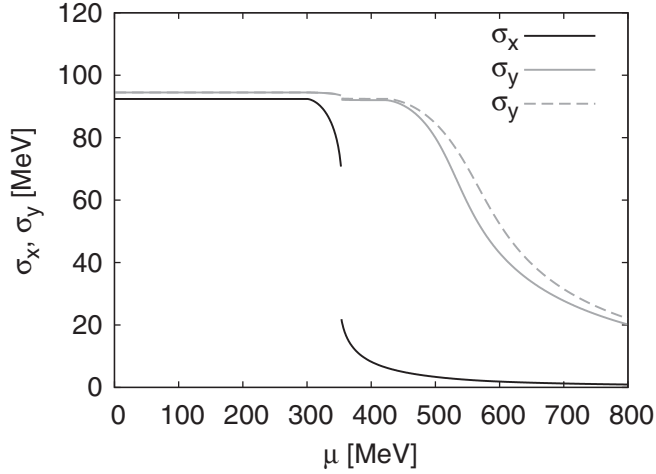
FIG. 2.   Similar to Fig. 1 but as a function of μ for $T = 0$.

ima and one maximum of the effective potential. Because of the explicit symmetry breaking both condensates remain always finite in the symmetric phase. The phase transition is mainly driven by the nonstrange condensate while the jump in the strange condensate is negligible. Above the transition for $\mu > \mu_c$ and below the strange Fermi surface at $\mu = m_s \sim 433$ MeV the strange condensate stays constant. The axial anomaly has almost no influence up to the strange quark Fermi surface. Only for chemical potentials larger than $\mu \sim 433$ MeV the strange condensate melts faster if the $U(1)_A$ symmetry breaking is taken into account. For large chemical potentials this difference vanishes again and both strange condensates will become identical. Furthermore, the in-medium behavior of the nonstrange condensate $\bar{\sigma}_x$ is not modified by the anomaly.

B. The scalar-pseudoscalar meson spectrum

In the following the in-medium scalar and pseudoscalar meson mass spectrum is analyzed. The derivation of the in-medium masses as well as the mass formulas are collected in Appendix B.

We start with the discussion of the mass spectrum at nonzero temperature and vanishing quark chemical potential. The meson masses as a function of the temperature for $\mu = 0$ are shown in Figs. 3 and 4. In the left panels of the respective figures the $U(1)_A$ symmetry breaking is explicitly taken into account while in the right panels the breaking is neglected.

The masses of the pion and the σ meson and also the masses of the η' and the a_0 meson degenerate approximately at the same temperature $T_c \sim 181$ MeV. This temperature behavior signals the effective restoration of chiral $SU(2) \times SU(2)$ symmetry in the nonstrange sector via a smooth crossover transition. The chiral partners (K, κ) show a similar temperature behavior but degenerate with the η meson at a higher temperature $T \sim 240$ MeV. At the chiral transition $T \sim 181$ MeV the κ meson becomes lighter than the a_0 meson. In contrast to [34] the η' is always heavier than the kaon for all temperatures. Only the $f_0(1370)$ meson mass does not show a tendency to converge to the η mass in the temperature region shown because chiral symmetry in the strange sector is restored only very slowly. The intersection point of the f_0 and the η mass coincides with the inflection point of the strange condensate. Nevertheless, the f_0 meson will degenerate with the remaining meson octet at very large temperatures.

The mass gap in the restored phase for $T > T_c$ between the two sets of the chiral partners, (σ, π) and (a_0, η'), i.e. $m_\pi = m_\sigma < m_{a_0} = m_{\eta'}$, is a consequence of the $U(1)_A$ breaking term. This gap is generated by an opposite sign
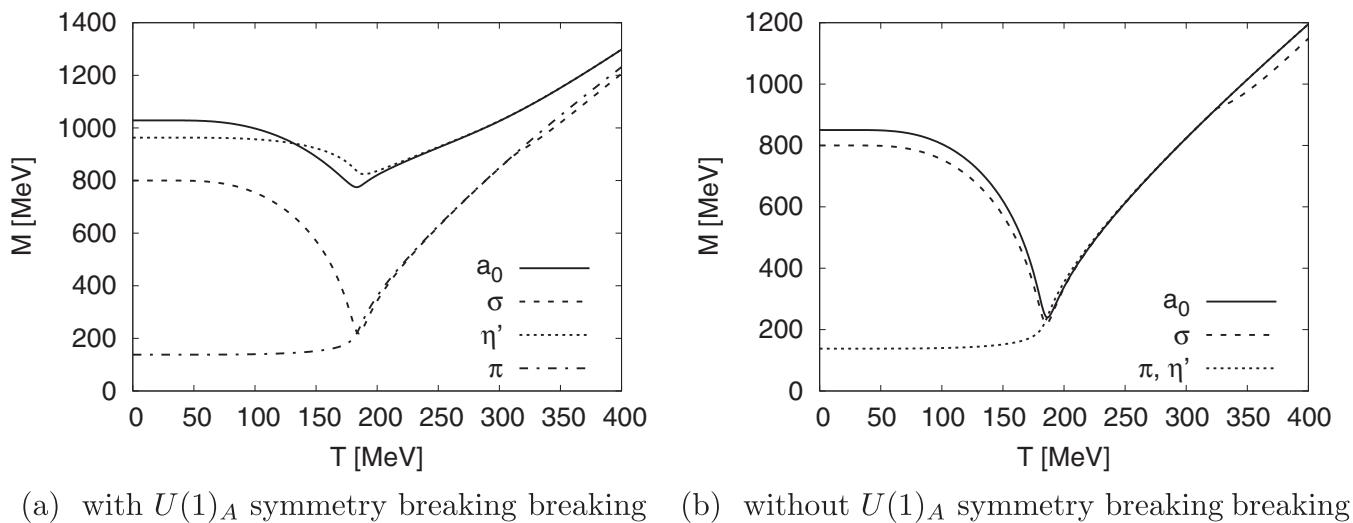

(a)   with $U(1)_A$ symmetry breaking breaking   (b)   without $U(1)_A$ symmetry breaking breaking

FIG. 3.   In-medium meson masses, (π, σ) and (η', a_0), as a function of temperature for $\mu = 0$ with $U(1)_A$ anomaly breaking (left panel). Without anomaly breaking (right panel) the η' meson degenerates with the pion mass. See text for further details.
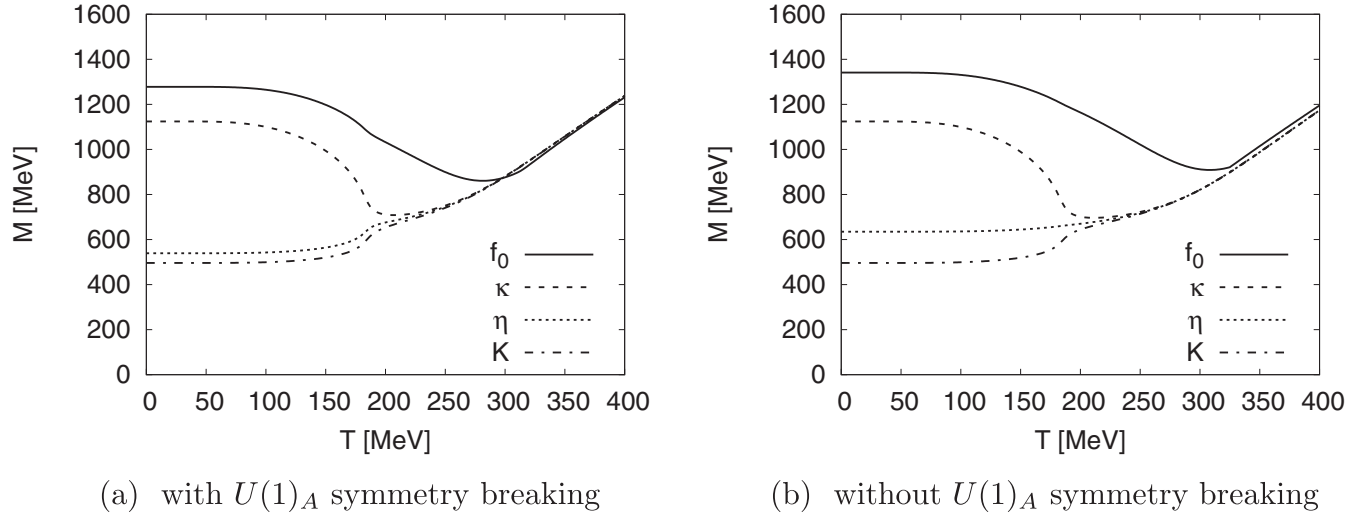
(a) with $U(1)_A$ symmetry breaking

(b) without $U(1)_A$ symmetry breaking

FIG. 4.   Similar to Fig. 3 for the chiral partners (η, f_0) and (K, κ) (left panel with $U(1)_A$ anomaly breaking). Without anomaly breaking (right panel) the η meson increases about 100 MeV in the vacuum.

of the anomaly term in the scalar and pseudoscalar meson masses, cf. Appendix B. It is basically given by $\sqrt{2}c\,\bar{\sigma}_y$, i.e. proportional to the anomaly term c and the strange order parameter $\bar{\sigma}_y$. The nonstrange condensate $\bar{\sigma}_x$ is already negligible for temperatures above T_c. For higher temperatures ($T \gg 400$ MeV) the $U(1)_A$ symmetry gets effectively restored and the mass gap between the chiral partners will vanish. Finally, for very large temperatures compared to the strange quark mass the difference between the strange and nonstrange mesons disappear and all meson masses will degenerate.

Without $U(1)_A$ symmetry breaking the mass gap between the chiral partners, (σ, π) and (a_0, η'), vanishes in the restored phase and all four meson masses degenerate at the same critical temperature $T_c \sim 181$ MeV coinciding with the inflection point of the nonstrange condensate. Above this temperature the axial symmetry is restored but the full restoration of the $U(3) \times U(3)$ symmetry is still not yet completed because the chiral partners (K, κ) degenerate with the η at a higher temperature $T \sim 240$ MeV. This temperature value and the value of T_c are not changed by the anomaly as expected since the nonstrange condensate is not influenced by the anomaly. Interestingly, a recent mean-field study within the three-flavor NJL model with various effective $U(1)_A$ anomaly implementations found an explicit difference for the chiral nonstrange transition temperatures with and without explicit $U(1)_A$ symmetry breaking (cf. Table III in [45]).

As for the case with anomaly, the chiral partners (η, f_0) degenerate but only for temperatures around 300 MeV because these mesons are purely strange states and chiral symmetry in the strange sector is very slowly restored. A mild anomaly dependence of the intersection point of the f_0 and the η meson is observed. There is no inverse mass ordering of the η meson and the kaon at finite temperature

as found in [34]. In the vacuum the mass of the f_0 increases by about 60 MeV if the anomaly is neglected.

Without the anomaly term the η' meson degenerates with the pion already in the vacuum and stays degenerated with the pion for all temperatures. Hence, in the vacuum the mass of the η' drops down considerably from 963 MeV to 138 MeV. In fact, it has been shown that the mass of the η' must be less then $\sqrt{3}m_\pi \sim 240$ MeV if the $U(1)_A$ symmetry is not explicitly broken [30].

In general, one can summarize the mass spectrum in-medium behavior in the following way: the bosonic thermal contributions decrease the meson masses while the fermionic parts increase the masses. For small temperatures the quark contribution is negligible and for high temperatures it dominates the mesonic contribution yielding rising and degenerate meson masses.

All meson masses are controlled by the two explicit symmetry breaking parameter h_x and h_y. They are determined by the tree-level Ward identities, Eq. (19), which guarantee the Goldstone theorem at zero temperature: for vanishing external parameter h_x the pion mass must also vanishes because f_π is then finite. In this case, the other symmetry breaking parameter h_y generates only a finite value for the kaon mass. Furthermore, the chiral limit can be reached by setting all explicit symmetry breaking parameters to zero. But in order to obtain finite vacuum expectation values for the condensates the symmetry must be spontaneously broken. This requires a negative m^2 parameter. Later, we will use several parameter fits for various values of the sigma meson mass which partly have a positive m^2 parameter (see Appendix A). For these parameter sets one cannot reach the chiral limit by just setting the explicit symmetry breaking parameters to zero. But these parameter sets are still well suited for fitting the physical mass point. For instance, choosing a

$m_\sigma = 400$ MeV the parameter fit results with or without anomaly in a positive m^2 parameter and the chiral limit cannot be reached for this parameter set. In [34] another strategy to investigate the chiral limit was adopted by performing a separate extra parameter fit where an average of the experimental mass values in the scalar octet spectrum together with some extrapolated quantities towards the chiral limit as input have been used. However, all in all the extrapolation towards the chiral limit remains questionable for both procedures.

For the parameter set with, e.g., $m_\sigma = 800$ MeV we can reach the chiral limit. For $c \neq 0$ we obtain a massless pseudoscalar octet and a finite $m_{\eta'} = 767$ MeV due to the $U(1)_A$ symmetry breaking. All scalar octet masses are degenerate at 840 MeV and the mass of the sigma meson drops down to 620 MeV. Moreover, without $U(1)_A$ symmetry breaking all nine pseudoscalar mesons are massless and the scalar octet masses are degenerated into 780 MeV and $m_\sigma = 712$ MeV.

In our approximation the Goldstone's theorem is also valid at finite temperature and chemical potentials, meaning that in the chiral limit the masses of the Goldstone bosons stay massless in the broken phase. Even in the presence of quarks both Ward identities in (19) are always fulfilled for all temperatures and quark chemical potentials which can be shown analytically.

Another observation in the Figs. 3 and 4 is the temperature behavior of the scalar σ and f_0 meson around $T \sim 325$ MeV. There is a kink visible in the curves and the meson masses seem to interchange their identities for higher temperatures. In order to elucidate this behavior we analyze the scalar and pseudoscalar mixing angles in the following.

C. Flavor mixing at finite temperature

The investigation of the mixing angles of the scalar and pseudoscalar isoscalar states provides further insights of the axial $U(1)_A$ symmetry restoration. In order to clarify our findings some underlying definitions and relations between different bases are given in Appendix C. Both mixing angles, the pseudoscalar θ_P and the scalar one θ_S, are shown in Fig. 5 as a function of temperature for $\mu = 0$ with and without explicit $U(1)_A$ symmetry breaking. In the broken phase, i.e. for $T < 200$ MeV, a strong influence of the anomaly on the pseudoscalar sector is found while almost no effect is seen in the scalar sector. With anomaly the nonstrange and strange quark states mix and generate an pseudoscalar mixing angle $\theta_P \sim -5°$ at $T = 0$. For increasing temperatures the mixing angle stays almost constant in the chirally broken phase. Around the chiral restoration temperature $T_c \sim 180$ MeV the angle increases smoothly towards the ideal mixing angle $\theta_P \to \arctan(1/\sqrt{2}) \sim +35°$ corresponding to $\phi_p = 90°$, where ϕ_p denotes the pseudoscalar mixing angle in the strange-nonstrange basis (see Appendix C for details). At high
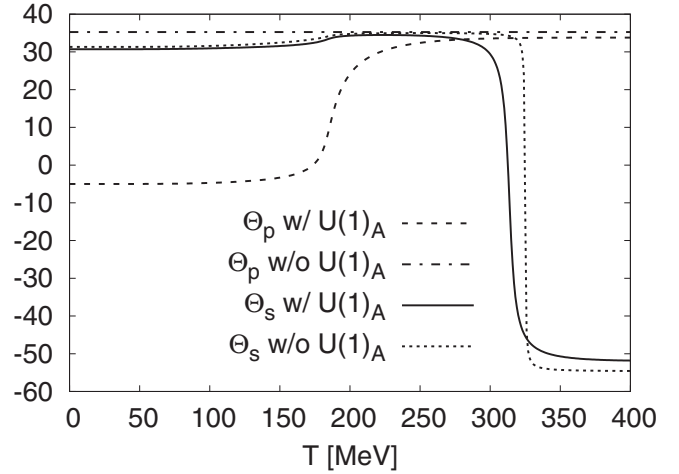

FIG. 5. The scalar θ_S and pseudoscalar θ_P mixing angles as a function of temperature for $\mu = 0$ without and with $U_A(1)$ anomaly.

temperatures this means that the η meson becomes a purely strange and the η' a purely nonstrange quark system (cf. [46]).

This is also demonstrated in Fig. 6 where the physical η-η' and the nonstrange-strange η_{NS}-η_S complex are shown as a function of temperature for $\mu = 0$. At $T = 0$ the nonstrange mass of the η_{NS} meson, $m_{\eta_{NS}}$, is larger than the strange mass m_{η_S} since the pseudoscalar mixing angle is larger than $\phi_p = 45°$, respectively $\theta_P = -9.74°$. For the mixing angle of $\theta_P \sim -5°$ ($\phi_p \sim 49.74°$) we obtain $m_{\eta_{NS}} \sim 813$ MeV and $m_{\eta_S} \sim 746$ MeV.

At the chiral transition temperature $T_c \sim 180$ MeV the η' meson becomes purely nonstrange ($\eta' \to \eta_{NS}$) while the η becomes a purely strange quark system ($\eta \to \eta_S$). In this temperature region the mixing angle grows to the ideal $\theta_P \to +35°$ (respectively $\phi_p \to 90°$). No crossing of the
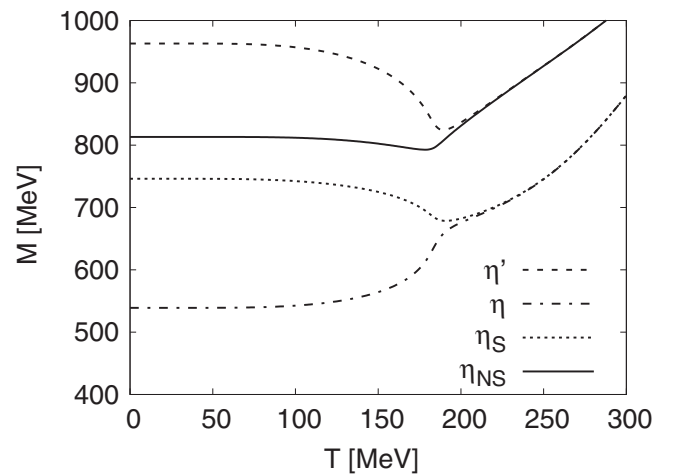

FIG. 6. Physical η-η' complex in comparison with the η_{NS}-η_S complex as a function of temperature at $\mu = 0$ with anomaly breaking.

η_{NS} and η_S or anticrossing[3] of the physical η-η' complex is observed for all temperatures since $\phi_p(T)$ is always above 45° [46].

Without anomaly the pseudoscalar mixing angle is already ideal for zero temperature and stays ideal for all temperatures, i.e. $\theta_P \sim +35°$. This means that already at $T = 0$ the η and η' mesons are ideally flavor-mixed. The η' is a purely light quark system and the η is a purely strange quark system. Without anomaly the η' degenerates in mass with the pion. Hence, the η' belongs to the class of nonstrange particles. The ordering of the corresponding nonstrange-strange masses is reversed, i.e. without anomaly m_{η_S} is larger than $m_{\eta_{NS}}$ since $m_{\eta_S} = m_\eta$ and $m_{\eta_{NS}} = m_{\eta'}$.

In the scalar sector the mixing angle θ_S shows no influence of the axial anomaly in the broken phase (see Fig. 5). In both cases, with and without anomaly breaking, the mixing angle is almost ideal $\theta_S \sim +31°$ at $T = 0$, but the precise vacuum value depends strongly on the value for the fitted scalar sigma meson mass in contrast to the pseudoscalar angle which is independent of m_σ, see Table II in Appendix A. For increasing m_σ the scalar mixing angle θ_S also increases at $T = 0$. As a consequence, for larger m_σ the nonstrange-strange σ_{NS}-σ_S complex and the physical σ and $f_0(1370)$ mesons degenerate more and more at $T = 0$, meaning that the σ meson tends to a pure nonstrange quark system, $\sigma \to \sigma_{NS}$, and the f_0 to a pure strange system, $f_0 \to \sigma_S$. For instance, we obtain for $m_\sigma(m_{f_0}) = 400(1257)$ MeV respectively $m_{\sigma_{NS}}(m_{\sigma_S}) = 561(1131)$ MeV and for $m_\sigma(m_{f_0}) = 800(1341)$ MeV $m_{\sigma_{NS}}(m_{\sigma_S}) = 804(1276)$ MeV.

At the chiral transition θ_S grows again to the ideal one. But for temperatures around $T \sim 314$ MeV in the chirally symmetric phase the scalar mixing angle drops down to $\theta_S \sim -54°$ ($\phi_s \sim 0°$). Around these temperature the masses of the physical σ and f_0 anticross and the ones of the nonstrange-strange σ_{NS}-σ_S system cross. This is displayed in Fig. 7. Hence, for larger temperatures, $T > 314$ MeV the f_0 is now a purely nonstrange quark system and the σ a purely strange state. For very large temperatures, around 900 MeV, the scalar mixing angle turns back to the ideal $\theta_S \sim +35°$ again and a crossing and anticrossing of the corresponding masses takes place again. Without anomaly the same phenomenon happens qualitatively around some larger temperatures of the order of $T \sim 325$ MeV.

For finite quark chemical potential and vanishing temperature the mixing angle shows qualitatively a similar behavior. Around $\mu \sim 350$ MeV the pseudoscalar angle θ_P increases towards the ideal value while without anomaly the angle is already ideal. In the scalar sector the angle

---

[3]A crossing of the η_{NS} and η_S masses corresponds to an anticrossing of the physical η and η' masses via Eqs. (C9) and (C10) (cf. also [47]).
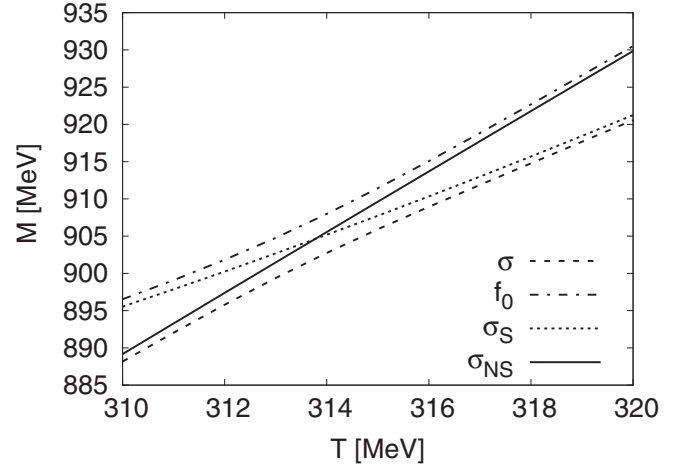
FIG. 7. Similar to Fig. 6: The scalar physical σ-f_0 complex around $T \sim 314$ MeV in comparison with the σ_{NS}-σ_S system with anomaly breaking.

is nearly ideal in the broken phase and drops down to $\theta_S \sim -54°$ around $\mu \sim 500$ MeV where again the masses of the physical σ and f_0 meson anticross.

A finite temperature study of the η-η' complex including the QCD axial anomaly within a Dyson-Schwinger approach and a temperature-dependent topological susceptibility can also be found in [47,48]. By means of the Witten-Veneziano relation the authors studied the interplay between the melting of the topological susceptibility and the chiral restoration temperature. The authors find a strong increase of the η' mass around the chiral restoration temperature which makes the extension of the Witten-Veneziano relation to finite temperature questionable. In the present work a constant anomaly parameter has been used corresponding to a constant topological susceptibility. This means that the $U(1)_A$ symmetry is not restored around the chiral critical temperature but at higher temperatures.

VI. PHASE DIAGRAM AND THE CHIRAL CRITICAL SURFACE

The phase diagram is constructed in the following way: for realistic pion and kaon masses (the so-called physical point) the light condensate melts always faster with T and/or μ than the strange condensate because the strange quark mass is heavier than the light quark mass. As the chiral phase boundary we use the inflection point in the light condensate.

Later on, we will also vary the meson masses and calculate the corresponding phase diagrams. As a consequence, the ordering of the light and strange condensates can be inverted since the kaon mass can become lighter than the pion mass. In such cases the strange condensate drops faster than the light condensate and the chiral phase transition is triggered by the strange condensate. This has to be taken into account systematically, in particular, for
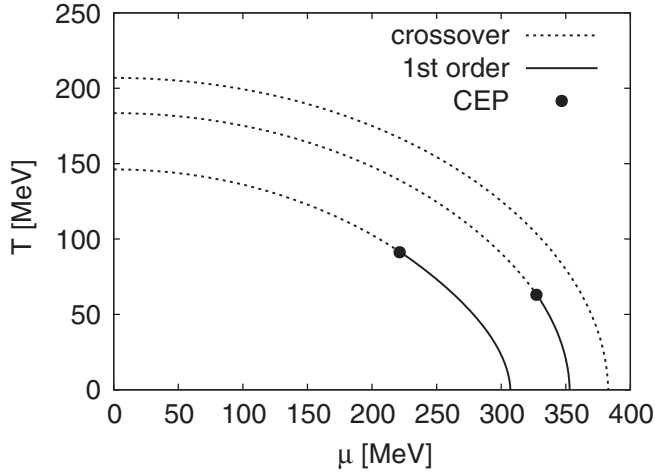
FIG. 8. Phase diagrams with $U(1)_A$ symmetry breaking for different values of $m_\sigma = 600$ MeV (lower line), 800 MeV, 900 MeV (upper line).

the calculation of the chiral critical surface. The faster melting condensate has been used in order to localize the phase boundary.

In Fig. 8 the phase diagrams in the (T, μ)-plane with explicit $U(1)_A$ symmetry breaking for three different values of m_σ are shown (lower lines correspond to $m_\sigma = 600$ MeV, next lines to $m_\sigma = 800$ MeV and upper lines to $m_\sigma = 900$ MeV). For each value of m_σ the remaining parameters of the model are fitted to the vacuum as described in Sec. IV and are kept constant. Since the explicit $U(1)_A$ symmetry breaking leads only to small modifications of the phase boundaries (cf. Figs. 1 and 2), we refrain from presenting the phase diagrams in the absence of an explicit $U(1)_A$ symmetry breaking term.

At zero chemical potential a crossover is always found due to the explicit symmetry breaking terms. The crossover temperature depends on the choice of the sigma meson mass. For increasing m_σ the pseudocritical temperature also increases (e.g., for $m_\sigma = 600$, 800, 900 MeV we found a $T_c \sim 146$, 184, 207 MeV).

Recent lattice simulations at $\mu = 0$ for three quark flavors have obtained values for the pseudocritical temperatures in the range of $T_c = 151(3)(3)$ MeV [14,49] and $T_c = 192(7)(4)$ MeV [11,50]. These results, applied to the current study, would suggest values for the sigma mass in between 600 and 800 MeV.

At zero temperature a first-order phase transition is obtained (cf. Fig. 2). For increasing temperatures the first-order transition becomes weaker and terminates in the critical end point (CEP). How to measure this point and what the distinctive signatures of this point are is not yet settled. It is interesting to see that the mass of the σ meson as a function of temperature and/or chemical potential through the CEP always drops below the mass of the pion not only for the corresponding two-flavor but also for the three-flavor calculation [22]. This is a general feature

of the LσM since the potential flattens at this point in radial σ direction. In a similar NJL calculation this is not the case [40,51].

For $m_\sigma = 600$ MeV the location of the CEP is at $(T_c, \mu_c) = (91, 221)$ MeV and for $m_\sigma = 800$ MeV at $(63, 327)$ MeV. As a consequence of the model parameters dependence, the location of the CEP moves for increasing m_σ towards the μ axis. It is interesting to observe that already for $m_\sigma = 900$ MeV the existence of the CEP disappears and the phase transition is a smooth crossover over the entire phase diagram.

Almost no influence of the axial anomaly on the phase boundaries and thus on the location of the CEP is seen. For comparison, with and without the $U(1)_A$ symmetry breaking and each for $m_\sigma = 600$ MeV the location of the CEP changes from $(T_c, \mu_c) = (91, 221)$ MeV to $(89, 228)$ MeV. For $m_\sigma = 800$ MeV the changes are even smaller $(T_c, \mu_c) = (63, 327)$ MeV to $(63, 328)$ MeV.

In Ref. [52] a gauged linear sigma model with chiral $U(N_f) \times U(N_f)$ symmetry without quarks within the 2PI resummation scheme has been considered. For the two-flavor case and neglecting the influence of the vector mesons the opposite behavior of the chiral phase transition as a function of m_σ is observed: for $\mu = 0$ a crossover is seen for a small σ mass ($m_\sigma = 441$ MeV) and a first-order transition for a large σ mass ($m_\sigma = 1370$ MeV). If the vector mesons are included the transition leads to a more rapid crossover and brings one closer to the second-order critical point. The conclusion is that the critical endpoint moves closer to the temperature axis. Thus, the inclusion of vector mesons should improve the agreement with lattice QCD results since usually, in chiral models, the critical endpoint is located at smaller temperatures and larger chemical potentials.

For three quark flavors renormalization-group arguments predict a first-order transition in the chiral limit independent of the $U(1)_A$ symmetry breaking [53]. This behavior is displayed in Fig. 9 where the resulting phase diagrams including the anomaly for varying pion and kaon masses are shown for $m_\sigma = 800$ MeV. We have chosen a path in the (m_π, m_K)-plane through the physical mass point towards the chiral limit by varying the pion mass and accordingly the kaon mass by keeping the ratio m_π/m_K fixed at the value given at the physical point m_π^*/m_K^*.

The pion and kaon masses are varied by changing the explicit symmetry breaking parameters, h_x and h_y, while keeping all remaining model parameters fixed at the values obtained at the physical point. For a pion mass 1.36 times larger than the physical one (for $m_\sigma = 800$ MeV) the CEP lies exactly on the μ-axis, hence for pion masses above this value the phase transition is a smooth crossover over the entire phase diagram and no CEP exists anymore.

For a decreasing pion mass, the location of the CEP moves towards the T-axis and already for half of the physical pion mass the CEP hits the T-axis at $\mu = 0$.
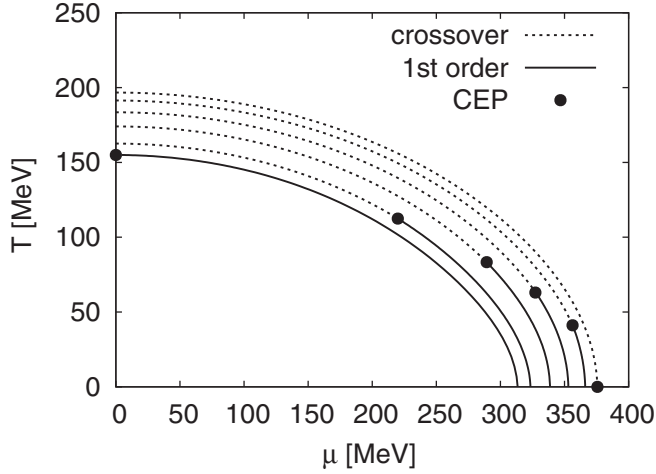
FIG. 9. Phase diagrams with $U(1)_A$ symmetry breaking for $m_\sigma = 800$ MeV and different pion masses: $m_\pi/m_\pi^* = 0.488$ (lower line), 0.6, 0.8, 1.0, 1.2, 1.36 (upper line), $m_\pi^* = 138$ MeV, $m_K^* = 496$ MeV. The ratio $m_\pi/m_K = m_\pi^*/m_K^*$ is kept fixed.

Remarkably also for half of the physical pion mass the CEP hits the T-axis in a similar calculation within a two-flavor LσM within the same approximation scheme but without $U(1)_A$ symmetry breaking and for $m_\sigma = 600$ MeV [22]. For smaller pion masses the chiral phase transition turns into a first-order one for all densities and consequently no CEP exists any longer.

The various transition lines in the phase diagram shrink towards the origin of the phase diagram for smaller pion and kaon masses because the condensates decrease more rapidly as a function of the temperature and chemical potentials. If one rescales the temperature with the critical temperature at $\mu = 0$ and the chemical potential with the critical chemical potential at $T = 0$ then all the transition

lines in the phase diagram lie on top of each other for different pion masses.

In connection with the existence of the CEP in the phase diagram it is interesting to analyze its mass sensitivity. For this purpose the critical surface for the chiral phase transition is evaluated in Fig. 10 as a function of the pion and the kaon masses with (left panel) and without (right panel) the $U(1)_A$ symmetry breaking. Again the masses are tuned by variation of only the explicit symmetry breaking parameters (see Eq. (19)) while keeping all other model parameters fixed similar to Ref. [54]. For small kaon masses but large pion masses the explicit symmetry breaking parameter for the strange direction h_y in Eq. (19) can become negative. The corresponding kaon mass, where this happens, is given by $m_K = m_\pi\sqrt{f_\pi/2f_K}$ and is shown in both panels as a solid line.

The critical surface is defined by the value of the critical chemical potential μ_c of the CEP for a given mass pair (m_π, m_K). It is the surface of the second-order phase transition points displayed in a three-dimensional (μ_c, m_π, m_K)-space. For values of the chemical potential above the chiral phase transition is of first-order while for values below the surface the transition lies in the crossover region. With or without anomaly the critical surface grows out perpendicular from the (m_π, m_K)-mass plane at $\mu = 0$. The tangent plane to the critical surface has a decreasing slope for larger masses as expected from Fig. 8 or Fig. 9. Thus, this model study excludes the so-called nonstandard scenario, found in a recent lattice analysis with imaginary chemical potentials, where the first-order region shrinks as the chemical potential is turned on [19]. In the nonstandard scenario the bending of the critical surface has the opposite sign and the physical realistic mass point remains in the crossover region for any μ. In Fig. 10 the physical mass point is denoted by an arrow. Since the critical chemical

(a) with $U(1)_A$ anomaly
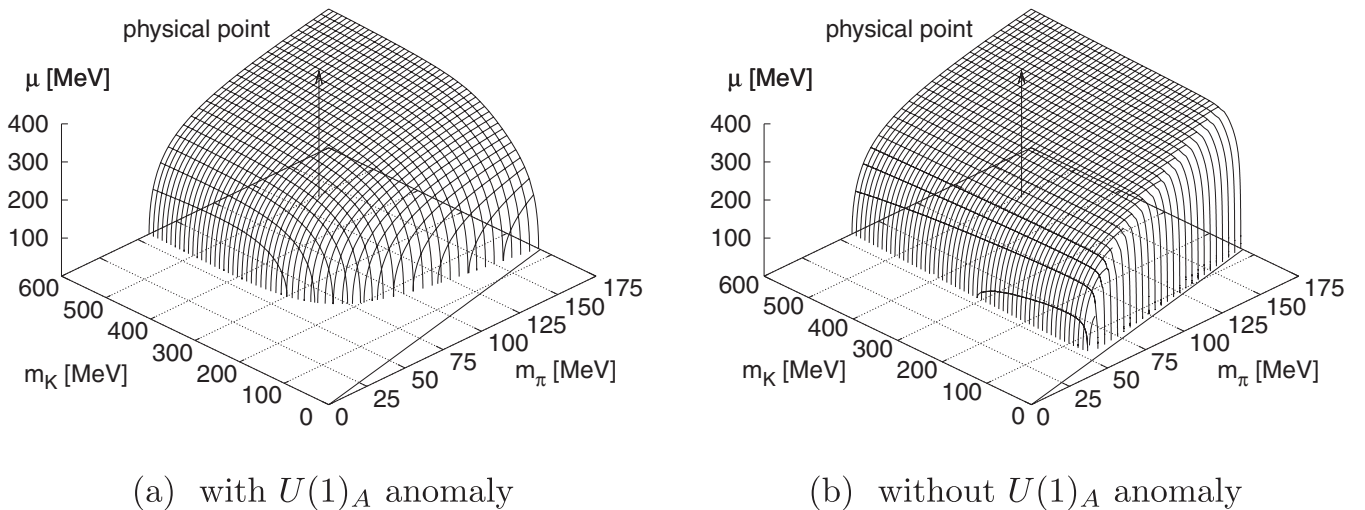
(b) without $U(1)_A$ anomaly

FIG. 10. The chiral critical surface in the (m_π, m_K) plane for $m_\sigma = 800$ MeV. The arrow points to the critical quark chemical potential at realistic pion and kaon masses (physical point). The solid line in the right panel is given by $m_K = m_\pi\sqrt{f_\pi/2f_K}$.

potential μ_c cannot grow arbitrarily the surface must have a boundary and hence stops to exist for larger (m_π, m_K)-masses which are not shown in the Figure.

In Ref. [39] the LσM with quarks in a one-loop approximation, based on optimized perturbation theory, was evaluated and a bending of the critical surface away from the m_K-axis at $m_\pi = 0$ for a kaon masses greater than 400 MeV was observed. The precise value of m_K for the onset of the bending depends on the order of the used chiral perturbation theory (χPT) for the baryon mass extrapolations. Thus, the unphysical bending indicates that the validity range of the χPT for the baryons, used for the model parameter extrapolation away from the physical point, was exceeded. As a consequence, no (tri)critical point on the m_K-axis for $\mu = 0$ where the boundary of the first-order transition region terminates can be located.

In this work no strong bending of the surface away from the m_K-axis is seen for kaon masses not larger than 600 MeV, but it also seems that it never approaches the m_K-axis at least for $m_\sigma = 800$ MeV. On the other hand, including the anomaly we find a critical $m_\pi^{\text{crit}} \sim 177$ MeV where the critical surface intersects the solid line in the left panel of Fig. 10. On this line and for $m_\pi > m_\pi^{\text{crit}}$ the transition turns into a smooth crossover. On the contrary, without anomaly (right panel in the figure), no critical pion mass is found at $\mu = 0$ at least for values below 200 MeV. This means that the phase transition on the solid line is still of first order similar to the findings of [54] where the influence of the anomaly on the phase transition for vanishing chemical potentials within a $SU(3) \times SU(3)$ LσM without fermions in Hartree approximation has been investigated.

Furthermore, the effect of the $U(1)_A$ anomaly on the shape of the surface is rather marginal for a kaon mass greater than 400 MeV (cf. both panels in Fig. 10). For larger kaon masses the strange sector decouples from the light sector and the chiral phase transition is basically driven by the (light) nonstrange particles.

On the other hand, for a kaon masses smaller than 400 MeV we see a considerable influence of the anomaly on the shape of the critical surface. Without anomaly the region of first-order phase transitions at $\mu = 0$ is reduced which is in contrast to the results obtained with a LσM without quarks [54]. In this reference, it is found that the first-order transition region at $\mu = 0$ grows with and without anomaly for increasing sigma masses. For sigma masses greater than 600 MeV and without anomaly the physical point is well located within the first-order region while it is always in the crossover region with anomaly.

Including quarks we obtain an opposite tendency: the physical point is always in the crossover region and for larger sigma masses the size of the first-order transition region at $\mu = 0$ decreases as can be seen from Fig. 11. In this figure five cross sections, for $m_\sigma = 500 \ldots 900$ MeV of the chiral critical surface with (left) and without anomaly (right panel), are shown as a function of the pion mass. As a trajectory in the (m_π, m_K)-plane a path through the physical point towards the chiral limit has been chosen for these figures. This path is given by fixing the pion over kaon mass ratio to the physical one, i.e. setting $m_K/m_\pi = m_K^*/m_\pi^*$ where the star denotes the corresponding physical masses.

For larger m_σ values the chiral critical surface with anomaly moves to smaller pion masses. This effect is less pronounced if the anomaly is neglected (right panel). In accordance with Fig. 8 the chiral critical surface line for $m_\sigma = 900$ MeV terminates before the physical point $(m_\pi/m_\pi^* = 1)$. Because of the positive m^2 parameter we cannot evaluate the chiral critical surface for arbitrary pion and kaon masses for smaller values of m_σ as already

(a) with $U(1)_A$ anomaly
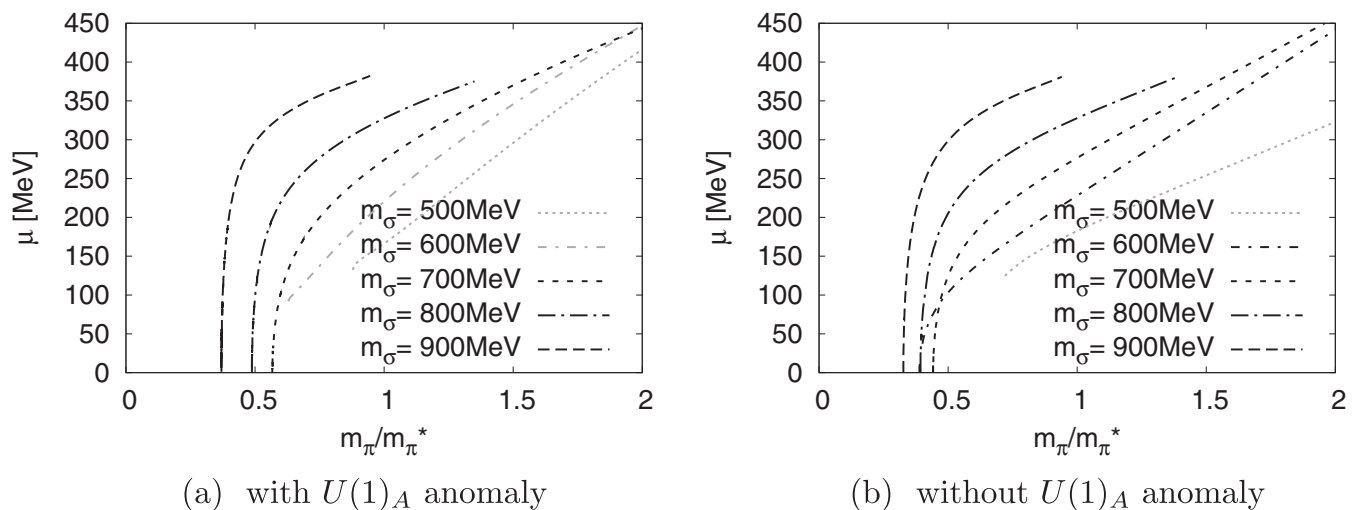
(b) without $U(1)_A$ anomaly

FIG. 11.   Five cross sections of the chiral critical surface (left panel with, right panel without anomaly) for $m_\sigma = 500, \ldots 900$ MeV. As trajectory in the (m_π, m_K) plane we have chosen the path through the physical point towards the chiral limit, i.e. we have kept the ratio of $m_\pi/m_K = m_\pi^*/m_K^*$ fixed. m_π^* and m_K^* denote the physical masses. See text for details.

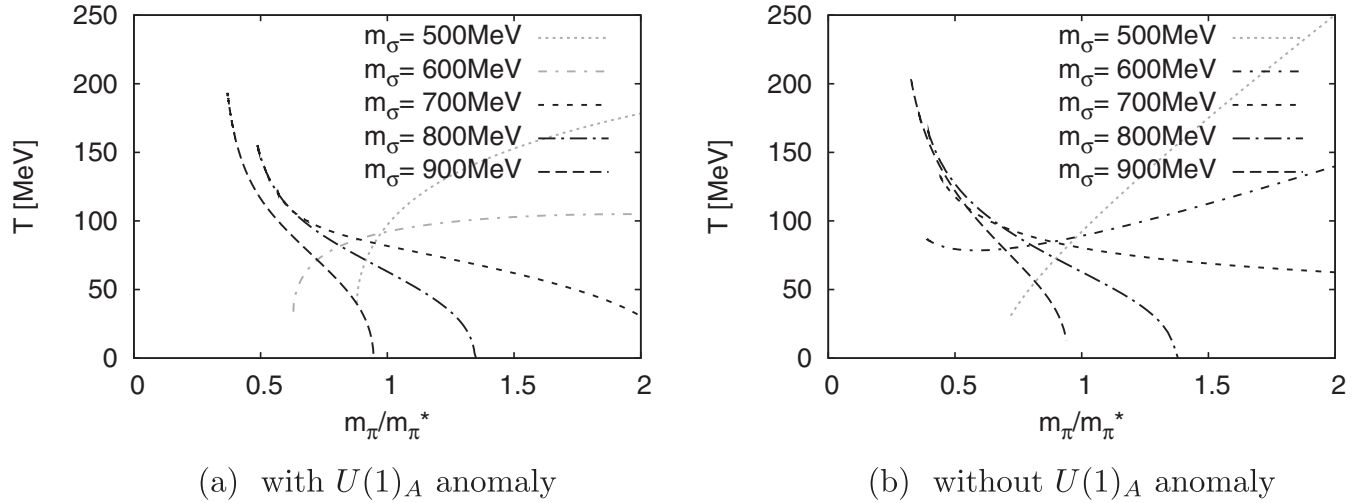(a) with $U(1)_A$ anomaly

(b) without $U(1)_A$ anomaly

FIG. 12.   Similar to Fig. 11 but the critical chemical potentials are replaced by the corresponding critical temperatures.

mentioned. Nevertheless, the results for smaller sigma masses are shown as dashed light curves in both panels and stop at certain pion mass ratios.

It is instructive to replace in the last Fig. 11 the critical chemical potential with the critical temperature and investigate its mass sensitivity. This leads to Fig. 12 where the critical temperatures of the CEP's as a function of the pion mass similar to Fig. 11 are plotted for five different σ meson masses with (left panel) and without anomaly (right panel). In general, the curves start at zero temperature and grow to a certain finite value for decreasing pion masses. For the parameter sets without spontaneous symmetry breaking the curves with anomaly for $m_\sigma = 500$ and 600 MeV, and without anomaly for $m_\sigma = 500$ MeV, show the opposite behavior. In this case, i.e. for smaller values of m_σ, and large unphysical pion masses $m_\pi/m_\pi^* > 1$, which is realized in lattice simulations, the location of the CEP moves towards the T-axis. For decreasing pion masses the critical temperatures decrease meaning that the CEP moves towards the μ-axis in the chiral limit. Consequently, for these parameter sets no first-order transition occurs in the chiral limit as already mentioned. Nevertheless, all of the curves intersect roughly at the physical point $(m_\pi/m_\pi^* = 1)$. Only the extrapolation towards the chiral limit is questionable as can be seen by the positive slope of these curves for decreasing pion masses.

VII. SUMMARY

In the present work chiral symmetry restoration in hot and dense hadronic matter is analyzed. As an effective realization of the spontaneous breaking of chiral symmetry in the vacuum, the $SU(3)_L \times SU(3)_R$ symmetric LσM with quarks has been used. Within this model, the grand thermodynamic potential was evaluated in the mean-field approximation. Six of the seven model parameters are fixed to the low-lying pseudoscalar mass spectrum, which is

experimentally well known and to the scalar sigma meson mass. Since the experimental situation in the scalar sector is not very certain we have varied the value of the sigma mass over a wide range and have investigated its consequences for the physics. The remaining model parameter, the Yukawa coupling, is determined by the nonstrange constituent quark mass while the condensates are governed by the PCAC relation.

At the physical mass point for various sigma masses a smooth finite temperature chiral crossover at zero density and a first-order transition for finite chemical potential at zero temperature is found. The $U(1)_A$ anomaly has only little influence on the strange condensate while no modification of the light condensate at the physical point is observed. The pseudocritical crossover temperature depends on the choice of the sigma meson mass and coincides with recent lattice simulations for mass values in between $m_\sigma = 600 \ldots 800$ MeV.

In our approximation no negative squared meson masses are generated in the medium as is the case for the LσM without quarks. Low-energy theorems like the Goldstone theorem or the Ward identities are not only fulfilled in the vacuum but also in the medium. This enables a careful analysis of the chiral symmetry restoration pattern of the meson nonets with and without axial anomaly. An anti-crossing of the scalar σ-$f_0(1370)$ masses at higher temperature is seen which is reflected in the corresponding mixing angle investigation.

For a sigma masses below 900 MeV a CEP is found in the phase diagram. In contrast to a similar calculation in the NJL model at this point the sigma meson mass drops below the pion mass. This behavior is analogous to the findings in the two-flavor case.

The chiral critical surface in the (m_π, m_K)-plane always has a positive slope such that the so-called nonstandard scenario can be excluded. In the chiral limit the expected first-order transition at $\mu = 0$ is found. A large modifica-

tion caused by the anomaly is visible. With anomaly the first-order region in the $\mu = 0$ plane is enlarged for smaller masses. For larger kaon masses the shape of the critical surface becomes independent of the anomaly. Furthermore, for increasing m_σ the surface becomes steeper.

One drawback of the effective model used here is the lack of confinement properties which certainly modify the thermodynamics in the broken phase. A first step towards an implementation of gluonic degrees of freedom which could mimic certain confinement aspects can be achieved by adding the Polyakov loop to the quark dynamics. Work in this direction is in progress [55].

APPENDIX A: PARAMETER FITS

In this appendix several used parameter fits for the linear sigma model (LσM) with three quark flavors are collected.

As experimental input we have chosen the low-lying pseudoscalar meson mass spectrum (m_π, m_K, m_η), the constituent quark mass m_q and the pion and kaon decay constant. To be more precise, for the fit with anomaly ($c \neq 0$) the sum $m_\eta^2 + m_{\eta'}^2$ is chosen as input while for $c = 0$ the m_η has not been used as input. The experimental values, taken from Ref. [42], are listed in the last line of Table II for comparison. Since the chiral σ-particle is a broad resonance its mass is not known precisely. We therefore have used different input values for m_σ in the range of 400–1000 MeV and have refitted the remaining parameters of the model accordingly. It is remarkable that larger sigma meson masses are not adjustable since m_σ as a function of the quartic coupling λ_1 saturates around 1100 MeV.

In Table II all resulting meson masses are listed. The upper block contains the fit without anomaly and the lower block the fit including the anomaly. Except for the pseudoscalar masses, the first four/five columns in the table respectively, all other (scalar) masses and the mixing angles are predictions of the model.

In Table I the values for the six mesonic model parameters of the LσM with and without explicit $U(1)_A$ symmetry breaking are summarized. The Yukawa coupling is always kept fixed to $g \sim 6.5$ corresponding to a constituent quark mass of $m_q = 300$ MeV. For this Yukawa coupling the strange constituent quark mass is predicted to be $m_s \approx 433$ MeV. The decay constants, $f_\pi = 92.4$ MeV and $f_K = 113$ MeV, are also kept constant for all fits. It is interesting to realize that for small values of m_σ and with $U(1)_A$ symmetry breaking the mass parameter m^2 changes

sign and becomes positive when fitted to realistic masses. As a consequence spontaneous symmetry breaking is lost in the chiral limit and all condensates will vanish in this limit. This happens for $m_\sigma \lesssim 700$ MeV. Even without anomaly breaking ($c = 0$) a similar phenomenon can be seen. For this case the masses are smaller when this case sets in, i.e. $m_\sigma \lesssim 500$ MeV. This is the motivation for our choice of $m_\sigma = 800$ MeV. For this parameter set we can investigate the mass sensitivity of the chiral phase transition over arbitrarily explicit symmetry breaking values including the chiral limit. The choice $m_\sigma = 800$ MeV for the parameter fit without anomaly is also in agreement with [34] where $m_\sigma = 600$ MeV is a misprint in this reference. For larger m_σ values the quartic coupling λ_1 increases significantly which restricts the parameter fits for m_σ larger than 1000 MeV.

APPENDIX B: MESON MASSES

The scalar $J^P = 0^+$ and pseudoscalar $J^P = 0^-$ meson masses are defined by the second derivative with respect to the corresponding scalar and pseudoscalar fields $\varphi_{s,a} = \sigma_a$ and $\varphi_{p,a} = \pi_a (a = 0, \ldots, 8)$ of the grand potential $\Omega(T, \mu_f)$, Eq. (7), evaluated at its minimum. The minimum is given by vanishing expectation values of all scalar and pseudoscalar fields but only two of them, $\bar{\sigma}_x$ and $\bar{\sigma}_y$, are nonzero.

$$m_{i,ab}^2 = \frac{\partial^2 \Omega(T, \mu_f)}{\partial \varphi_{i,a} \partial \varphi_{i,b}} \bigg|_{\min}; \qquad i = s, p. \quad \text{(B1)}$$

In the vacuum the contribution from the quark potential vanishes. Hence, only the mesonic part of the potential determines the mass matrix completely. The squared mass matrix is diagonal and due to isospin $SU(2)$ symmetry several matrix entries are degenerate. We begin with the scalar, $J^P = 0^+$, sector corresponding to $i = s$. The squared mass of the a_0 meson is given by the (11) element which is degenerate with the (22) and (33) elements. Similar, the squared κ meson mass is given by the (44) element which is also degenerated with the (55), (66) and (77) elements. The σ and $f_0(1370)$ meson masses are obtained by diagonalizing the (00)–(88) sector of the mass matrix introducing in this way a mixing angle θ_S. Explicitly, the squared masses for scalar sector, formulated in the nonstrange-strange basis, are

$$m_{a_0}^2 = m^2 + \lambda_1(\bar{\sigma}_x^2 + \bar{\sigma}_y^2) + \frac{3\lambda_2}{2}\bar{\sigma}_x^2 + \frac{\sqrt{2}c}{2}\bar{\sigma}_y, \quad \text{(B2)}$$

$$m_\kappa^2 = m^2 + \lambda_1(\bar{\sigma}_x^2 + \bar{\sigma}_y^2) + \frac{\lambda_2}{2}(\bar{\sigma}_x^2 + \sqrt{2}\bar{\sigma}_x\bar{\sigma}_y + 2\bar{\sigma}_y^2)$$
$$+ \frac{c}{2}\bar{\sigma}_x, \quad \text{(B3)}$$

$$m_\sigma^2 = m_{s,00}^2\cos^2\theta_S + m_{s,88}^2\sin^2\theta_S + 2m_{s,08}^2\sin\theta_S\cos\theta_S, \tag{B4}$$

$$m_{f_0}^2 = m_{s,00}^2\sin^2\theta_S + m_{s,88}^2\cos^2\theta_S - 2m_{s,08}^2\sin\theta_S\cos\theta_S \tag{B5}$$

with

$$m_{s,00}^2 = m^2 + \frac{\lambda_1}{3}(7\bar\sigma_x^2 + 4\sqrt{2}\bar\sigma_x\bar\sigma_y + 5\bar\sigma_y^2)$$
$$+ \lambda_2(\bar\sigma_x^2 + \bar\sigma_y^2) - \frac{\sqrt{2}c}{3}(\sqrt{2}\bar\sigma_x + \bar\sigma_y),$$

$$m_{s,88}^2 = m^2 + \frac{\lambda_1}{3}(5\bar\sigma_x^2 - 4\sqrt{2}\bar\sigma_x\bar\sigma_y + 7\bar\sigma_y^2)$$
$$+ \lambda_2\left(\frac{\bar\sigma_x^2}{2} + 2\bar\sigma_y^2\right) + \frac{\sqrt{2}c}{3}\left(\sqrt{2}\bar\sigma_x - \frac{\bar\sigma_y}{2}\right), \tag{B6}$$

$$m_{s,08}^2 = \frac{2\lambda_1}{3}(\sqrt{2}\bar\sigma_x^2 - \bar\sigma_x\bar\sigma_y - \sqrt{2}\bar\sigma_y^2) + \sqrt{2}\lambda_2\left(\frac{\bar\sigma_x^2}{2} - \bar\sigma_y^2\right)$$
$$+ \frac{c}{3\sqrt{2}}(\bar\sigma_x - \sqrt{2}\bar\sigma_y).$$

The situation for the pseudoscalar sector ($i = p$) is completely analogous with the following labeling: the squared pion mass is identified with the (11) element and the squared kaon mass with the (44) element of the pseudoscalar mass matrix. Similar to the scalar case, the η and η' mass are obtained by diagonalizing the (00)–(88) sector and accordingly a pseudoscalar mixing angle θ_P is introduced. Explicitly, the squared masses for the pseudoscalar sector are

$$m_\pi^2 = m^2 + \lambda_1(\bar\sigma_x^2 + \bar\sigma_y^2) + \frac{\lambda_2}{2}\bar\sigma_x^2 - \frac{\sqrt{2}c}{2}\bar\sigma_y \tag{B7}$$

$$m_K^2 = m^2 + \lambda_1(\bar\sigma_x^2 + \bar\sigma_y^2) + \frac{\lambda_2}{2}(\bar\sigma_x^2 - \sqrt{2}\bar\sigma_x\bar\sigma_y + 2\bar\sigma_y^2)$$
$$- \frac{c}{2}\bar\sigma_x \tag{B8}$$

$$m_{\eta'}^2 = m_{p,00}^2\cos^2\theta_P + m_{p,88}^2\sin^2\theta_P + 2m_{p,08}^2\sin\theta_P\cos\theta_P \tag{B9}$$

$$m_\eta^2 = m_{p,00}^2\sin^2\theta_P + m_{p,88}^2\cos^2\theta_P - 2m_{p,08}^2\sin\theta_P\cos\theta_P \tag{B10}$$

with

$$m_{p,00}^2 = m^2 + \lambda_1(\bar\sigma_x^2 + \bar\sigma_y^2) + \frac{\lambda_2}{3}(\bar\sigma_x^2 + \bar\sigma_y^2)$$
$$+ \frac{c}{3}(2\bar\sigma_x + \sqrt{2}\bar\sigma_y)$$

$$m_{p,88}^2 = m^2 + \lambda_1(\bar\sigma_x^2 + \bar\sigma_y^2) + \frac{\lambda_2}{6}(\bar\sigma_x^2 + 4\bar\sigma_y^2)$$
$$- \frac{c}{6}(4\bar\sigma_x - \sqrt{2}\bar\sigma_y)$$

$$m_{p,08}^2 = \frac{\sqrt{2}\lambda_2}{6}(\bar\sigma_x^2 - 2\bar\sigma_y^2) - \frac{c}{6}(\sqrt{2}\bar\sigma_x - 2\bar\sigma_y).$$

Both mixing angles are given by

$$\tan 2\Theta_i = \frac{2m_{i,08}^2}{m_{i,00}^2 - m_{i,88}^2}, \qquad i = s, p. \tag{B11}$$

In the medium the meson masses are further modified by the quark contribution (8). In order to evaluate the second derivate (B1) for the quark contribution the complete dependence of all scalar and pseudoscalar meson fields, cf. Eq. (3), in the quark masses has to be taken into account. The resulting quark mass matrix can be diagonalized. Finally, we obtain the expression

$$\frac{\partial^2\Omega_{\bar qq}(T, \mu_f)}{\partial\varphi_{i,\alpha}\partial\varphi_{i,\beta}}\bigg|_{\min} = \nu_c\sum_{f=q,s}\int\frac{d^3p}{(2\pi)^3}\frac{1}{2E_{q,f}}$$
$$\times\left[(n_{q,f} + n_{\bar q,f})\left(m_{f,\alpha\beta}^2 - \frac{m_{f,\alpha}^2 m_{f,\beta}^2}{2E_{q,f}^2}\right)\right.$$
$$\left. - \frac{(b_{q,f} + b_{\bar q,f})}{2E_{q,f}T}m_{f,\alpha}^2 m_{f,\beta}^2\right] \tag{B12}$$

where we have introduced the shorthand notation $m_{f,a}^2 \equiv \partial m_f^2/\partial\varphi_{i,a}$ for the quark mass derivative with respect to the meson fields $\varphi_{i,a}$, the quark function

$$b_{q,f}(T, \mu_f) = n_{q,f}(T, \mu_f)(1 - n_{q,f}(T, \mu_f)) \tag{B13}$$

TABLE III. Squared quark mass second derivatives with respect to the meson fields evaluated at the minimum. Left column block, the sum over two light quark flavors, denoted by index l, and right column block only the strange quark flavor, index s.

	$m_{l,\alpha}^2 m_{l,\beta}^2/g^4$	$m_{l,\alpha\beta}^2/g^2$	$m_{s,\alpha}^2 m_{s,\beta}^2/g^4$	$m_{s,\alpha\beta}^2/g^2$
$\bar\sigma_0\,\bar\sigma_0$	$\frac{1}{3}\bar\sigma_x^2$	$\frac{2}{3}$	$\frac{1}{3}\bar\sigma_y^2$	$\frac{1}{3}$
$\bar\sigma_1\,\bar\sigma_1$	$\frac{1}{2}\bar\sigma_x^2$	1	0	0
$\bar\sigma_4\,\bar\sigma_4$	0	$\bar\sigma_x\frac{\bar\sigma_x + \sqrt{2}\bar\sigma_y}{\bar\sigma_x^2 - 2\bar\sigma_y^2}$	0	$\bar\sigma_y\frac{\sqrt{2}\bar\sigma_x + 2\bar\sigma_y}{2\bar\sigma_y^2 - \bar\sigma_x^2}$
$\bar\sigma_8\,\bar\sigma_8$	$\frac{1}{6}\bar\sigma_x^2$	$\frac{1}{3}$	$\frac{2}{3}\bar\sigma_y^2$	$\frac{2}{3}$
$\bar\sigma_0\,\bar\sigma_8$	$\frac{\sqrt{2}}{6}\bar\sigma_x^2$	$\frac{\sqrt{2}}{3}$	$-\frac{\sqrt{2}}{3}\bar\sigma_y^2$	$-\frac{\sqrt{2}}{3}$
$\pi_0\,\pi_0$	0	$\frac{2}{3}$	0	$\frac{1}{3}$
$\pi_1\,\pi_1$	0	1	0	0
$\pi_4\,\pi_4$	0	$\bar\sigma_x\frac{\bar\sigma_x - \sqrt{2}\bar\sigma_y}{\bar\sigma_x^2 - 2\bar\sigma_y^2}$	0	$\bar\sigma_y\frac{\sqrt{2}\bar\sigma_x - 2\bar\sigma_y}{\bar\sigma_x^2 - 2\bar\sigma_y^2}$
$\pi_8\,\pi_8$	0	$\frac{1}{3}$	0	$\frac{2}{3}$
$\pi_0\,\pi_8$	0	$\frac{\sqrt{2}}{3}$	0	$-\frac{\sqrt{2}}{3}$

and correspondingly the antiquark function $b_{\bar{q},f}(T, \mu_f) = b_{q,f}(T, -\mu_f)$. The index i distinguishes between a scalar and pseudoscalar field which we omit in the following. In Table III all second quark mass derivatives with respect to the meson fields replaced by the nonvanishing vacuum expectation values in the nonstrange-strange basis are collected. Despite the $SU(2)$ isospin symmetry the derivatives are different for the up- and down-quark sector. In the Table III, left column block, the sum over the two light quark flavors is shown which leads to large cancellations.

APPENDIX C: ISOSCALAR MIXING

In this appendix a collection of relations describing the mixing of isoscalar states in the pseudoscalar and scalar multiplet is presented. The isoscalar ($I = 0$) pseudoscalar states in the octet-singlet (η_8, η_0) basis are defined by

$$|\eta_8\rangle = \frac{1}{\sqrt{6}}|u\bar{u} + d\bar{d} - 2s\bar{s}\rangle,$$
$$|\eta_0\rangle = \frac{1}{\sqrt{3}}|u\bar{u} + d\bar{d} + s\bar{s}\rangle. \tag{C1}$$

For a realistic flavor breaking in the vacuum the physical η meson is close to the η_8 and η' to η_0.

The eigenstates in the flavor nonstrange-strange (η_{NS}, η_{S}) basis are given by

$$|\eta_{\mathrm{NS}}\rangle = \frac{1}{\sqrt{2}}|u\bar{u} + d\bar{d}\rangle, \qquad |\eta_{\mathrm{S}}\rangle = |s\bar{s}\rangle. \tag{C2}$$

These states are associated to each other by a rotation with an angle $\alpha = -\arctan\sqrt{2} \sim -54.74°$

$$\begin{pmatrix} |\eta_{\mathrm{NS}}\rangle \\ |\eta_{\mathrm{S}}\rangle \end{pmatrix} = \frac{1}{\sqrt{3}} \begin{pmatrix} 1 & \sqrt{2} \\ -\sqrt{2} & 1 \end{pmatrix} \begin{pmatrix} |\eta_8\rangle \\ |\eta_0\rangle \end{pmatrix}. \tag{C3}$$

Diagonalization of the mass matrix in the (η_8, η_0) basis is achieved by the introduction of the pseudoscalar mixing angle θ_P. This yields the relations

$$\begin{pmatrix} |\eta\rangle \\ |\eta'\rangle \end{pmatrix} = \begin{pmatrix} \cos\theta_P & -\sin\theta_P \\ \sin\theta_P & \cos\theta_P \end{pmatrix} \begin{pmatrix} |\eta_8\rangle \\ |\eta_0\rangle \end{pmatrix}. \tag{C4}$$

For the (η_{NS}, η_{S}) basis a similar relation with the mixing angle ϕ_p holds

$$\begin{pmatrix} |\eta\rangle \\ |\eta'\rangle \end{pmatrix} = \begin{pmatrix} \cos\phi_p & -\sin\phi_p \\ \sin\phi_p & \cos\phi_p \end{pmatrix} \begin{pmatrix} |\eta_{\mathrm{NS}}\rangle \\ |\eta_{\mathrm{S}}\rangle \end{pmatrix}. \tag{C5}$$

For vanishing mixing angle ϕ_p corresponding to $\theta_P = -\arctan\sqrt{2} \sim -54,7°$ the η tends to a pure nonstrange η_{NS} and η' to a pure strange η_{S}. In contrast, for a mixing angle $\phi_p = 90°$ ($\theta_P \sim +35,3°$) the ordering is reversed and $\eta \to \eta_{\mathrm{S}}$ and $\eta' \to \eta_{\mathrm{NS}}$. The ordering transition occurs at $\phi_p = 45°$ ($\theta_P \sim -9.74°$).

The diagonalization of the mass matrix in the (η_{NS}, η_{S}) basis leads to the masses

$$m_\eta^2 = m_{\eta_{\mathrm{NS}}}^2\cos^2\phi_p + m_{\eta_{\mathrm{S}}}^2\sin^2\phi_p - m_{\eta_{\mathrm{S}},\eta_{\mathrm{NS}}}^2\sin^2(2\phi_p), \tag{C6}$$

$$m_{\eta'}^2 = m_{\eta_{\mathrm{NS}}}^2\sin^2\phi_p + m_{\eta_{\mathrm{S}}}^2\cos^2\phi_p + m_{\eta_{\mathrm{S}},\eta_{\mathrm{NS}}}^2\sin^2(2\phi_p), \tag{C7}$$

and to the mixing angle ϕ_p given by

$$\tan2\phi_p = \frac{2m_{\eta_{\mathrm{S}},\eta_{\mathrm{NS}}}^2}{m_{\eta_{\mathrm{S}}}^2 - m_{\eta_{\mathrm{NS}}}^2}. \tag{C8}$$

Equivalently, these expressions can be rewritten in a form which does not contain the mixing angle explicitly

$$m_{\eta'}^2 = \frac{1}{2}(m_{\eta_{\mathrm{NS}}}^2 + m_{\eta_{\mathrm{S}}}^2 + \Delta_{\eta_{\mathrm{NS}},\eta_{\mathrm{S}}}), \tag{C9}$$

$$m_\eta^2 = \frac{1}{2}(m_{\eta_{\mathrm{NS}}}^2 + m_{\eta_{\mathrm{S}}}^2 - \Delta_{\eta_{\mathrm{NS}},\eta_{\mathrm{S}}}), \tag{C10}$$

with $\Delta_{\eta_{\mathrm{NS}},\eta_{\mathrm{S}}} \equiv \sqrt{(m_{\eta_{\mathrm{NS}}}^2 - m_{\eta_{\mathrm{S}}}^2)^2 + 4m_{\eta_{\mathrm{NS}},\eta_{\mathrm{S}}}^2}$. Note, that these expressions are numerically more stable compared to (C6) and (C7) because possible ambiguities in the tangent (C8) do not appear here.

The matrix elements in the (η_{NS}, η_{S}) system are obtained by a base change from the ones in the (η_8, η_0) basis with the result

$$m_{\eta_{\mathrm{NS}}}^2 = \frac{1}{3}(2m_{p,00}^2 + m_{p,88}^2 + 2\sqrt{2}m_{p,08}^2),$$
$$m_{\eta_{\mathrm{S}}}^2 = \frac{1}{3}(m_{p,00}^2 + 2m_{p,88}^2 - 2\sqrt{2}m_{p,08}^2), \tag{C11}$$
$$m_{\eta_{\mathrm{S}},\eta_{\mathrm{NS}}}^2 = \frac{1}{3}(\sqrt{2}(m_{p,00}^2 - m_{p,88}^2) - m_{p,08}^2).$$

As a consequence, the mixing angles ϕ_p and θ_P are related by

$$\phi_p = \theta_P + \arctan\sqrt{2} \sim \theta_P + 54.74°. \tag{C12}$$

Furthermore, supposing $m_\eta \le m_{\eta'}$ one finds with (C6) and (C7) for $\phi_p \le 45°$ ($\theta_P \le -9.74°$) $m_{\eta_{\mathrm{NS}}} \le m_{\eta_{\mathrm{S}}}$ while for $\phi_p > 45°$ the ordering of the masses in the nonstrange-strange system are reversed.

Scalar mesons differ from the pseudoscalar ones only in the orbital excitation. Hence, all quoted relations can be immediately converted to the scalar (σ, f_0) complex with the corresponding replacements, e.g.,

$$\begin{pmatrix} |f_0\rangle \\ |\sigma\rangle \end{pmatrix} = \begin{pmatrix} \cos\phi_s & -\sin\phi_s \\ \sin\phi_s & \cos\phi_s \end{pmatrix} \begin{pmatrix} |\sigma_{\mathrm{NS}}\rangle \\ |\sigma_{\mathrm{S}}\rangle \end{pmatrix}. \tag{C13}$$

For an ideal scalar mixing angle $\phi_s = 90°$ the σ meson is a pure nonstrange state σ_{NS} and $f_0 \to -\sigma_{\mathrm{S}}$. Furthermore, σ matches with η' and f_0 with η.

Since the mass of the f_0 meson is larger than m_σ we obtain for an ideal mixing $\phi_s = 90°$ the ordering $m_{\sigma_{\mathrm{S}}} > m_{\sigma_{\mathrm{NS}}}$.

[1] B. Svetitsky, Phys. Rep. **132**, 1 (1986); H. Meyer-Ortmanns, Rev. Mod. Phys. **68**, 473 (1996); D. H. Rischke, Prog. Part. Nucl. Phys. **52**, 197 (2004).

[2] M. A. Stephanov, Proc. Sci., LAT2006 (2006) 024; M. A. Stephanov, Prog. Theor. Phys. Suppl. **153**, 139 (2004).

[3] S. P. Klevansky, Rev. Mod. Phys. **64**, 649 (1992); T. Hatsuda and T. Kunihiro, Phys. Rep. **247**, 221 (1994); M. Buballa, Phys. Rep. **407**, 205 (2005).

[4] P. N. Meisinger and M. C. Ogilvie, Phys. Lett. B **379**, 163 (1996).

[5] K. Fukushima, Phys. Lett. B **591**, 277 (2004).

[6] C. Ratti, M. A. Thaler, and W. Weise, Phys. Rev. D **73**, 014019 (2006); E. Megias, E. Ruiz Arriola, and L. L. Salcedo, Phys. Rev. D **74**, 065005 (2006); B.-J. Schaefer, J. M. Pawlowski, and J. Wambach, Phys. Rev. D **76**, 074023 (2007); C. Sasaki, B. Friman, and K. Redlich, Phys. Rev. D **75**, 074013 (2007); H. Abuki, R. Anglani, R. Gatto, G. Nardulli, and M. Ruggieri, Phys. Rev. D **78**, 034034 (2008); K. Fukushima, Phys. Rev. D **77**, 114028 (2008); **77**, 039902(E), (2008).

[7] M. Asakawa and K. Yazaki, Nucl. Phys. **A504**, 668 (1989); A. Barducci, R. Casalbuoni, S. De Curtis, R. Gatto, and G. Pettini, Phys. Lett. B **231**, 463 (1989); A. Barducci, R. Casalbuoni, G. Pettini, and R. Gatto, Phys. Rev. D **49**, 426 (1994); M. A. Stephanov, K. Rajagopal, and E. V. Shuryak, Phys. Rev. Lett. **81**, 4816 (1998); M. A. Halasz, A. D. Jackson, R. E. Shrock, M. A. Stephanov, and J. J. M. Verbaarschot, Phys. Rev. D **58**, 096007 (1998); J. Berges and K. Rajagopal, Nucl. Phys. **B538**, 215 (1999).

[8] F. Karsch, Lect. Notes Phys. **583**, 209 (2002).

[9] Z. Fodor, S. D. Katz, and K. K. Szabo, Phys. Lett. B **568**, 73 (2003).

[10] C. R. Allton, M. Doering, S. Ejiri, S. J. Hands, O. Kaczmarek, F. Karsch, E. Laermann, and K. Redlich, Phys. Rev. D **71**, 054508 (2005).

[11] Y. Aoki, Z. Fodor, S. D. Katz, and K. K. Szabo, Phys. Lett. B **643**, 46 (2006).

[12] F. Karsch, J. Phys. G **31**, S633 (2005).

[13] F. Karsch, arXiv:hep-ph/0701210.

[14] M. Cheng *et al.*, Phys. Rev. D **74**, 054507 (2006).

[15] M. Cheng *et al.*, Phys. Rev. D **77**, 014511 (2008).

[16] P. de Forcrand and O. Philipsen, Nucl. Phys. **B673**, 170 (2003).

[17] M. D'Elia and M. P. Lombardo, Phys. Rev. D **70**, 074509 (2004).

[18] M. D'Elia and M.-P. Lombardo, Phys. Rev. D **67**, 014505 (2003).

[19] P. de Forcrand and O. Philipsen, J. High Energy Phys. 01 (2007) 077.

[20] P. de Forcrand, S. Kim, and O. Philipsen, Proc. Sci., LAT2007 (2007) 178.

[21] O. Philipsen, Eur. Phys. J. Spec. Top. **152**, 29 (2007).

[22] B.-J. Schaefer and J. Wambach, Phys. Rev. D **75**, 085015 (2007).

[23] B.-J. Schaefer and J. Wambach, Nucl. Phys. **A757**, 479 (2005).

[24] E. Witten, Nucl. Phys. **B156**, 269 (1979); G. Veneziano, Nucl. Phys. **B159**, 213 (1979).

[25] R. Alkofer, C. S. Fischer, and R. Williams, arXiv:0804.3478.

[26] M. Gell-Mann and M. Levy, Nuovo Cimento **16**, 705 (1960).

[27] D. W. McKay, W. F. Palmer, and R. F. Sarraga, Phys. Rev. D**8**, 2532 (1973).

[28] H. Pagels, Phys. Rep. **16**, 219 (1975).

[29] S. Gasiorowicz and D. A. Geffen, Rev. Mod. Phys. **41**, 531 (1969).

[30] S. Weinberg, Phys. Rev. D **11**, 3583 (1975).

[31] H. Goldberg, Phys. Lett. B **131**, 133 (1983).

[32] H. Meyer-Ortmanns, H. J. Pirner, and A. Patkos, Phys. Lett. B **295**, 255 (1992).

[33] H. Meyer-Ortmanns and B.-J. Schaefer, Phys. Rev. D **53**, 6586 (1996).

[34] J. T. Lenaghan, D. H. Rischke, and J. Schaffner-Bielich, Phys. Rev. D **62**, 085008 (2000).

[35] D. Roder, J. Ruppert, and D. H. Rischke, Phys. Rev. D **68**, 016003 (2003).

[36] J. Schaffner-Bielich and J. Randrup, Phys. Rev. C **59**, 3329 (1999).

[37] S. Chiku and T. Hatsuda, Phys. Rev. D **58**, 076001 (1998).

[38] T. Herpay, A. Patkos, Z. Szep, and P. Szepfalusy, Phys. Rev. D **71**, 125017 (2005); T. Herpay and Z. Szep, Phys. Rev. D **74**, 025008 (2006); P. Kovacs and Z. Szep, Phys. Rev. D **77**, 065016 (2008).

[39] P. Kovacs and Z. Szep, Phys. Rev. D **75**, 025015 (2007).

[40] O. Scavenius, A. Mocsy, I. N. Mishustin, and D. H. Rischke, Phys. Rev. C **64**, 045202 (2001).

[41] J. Kapusta, *Finite-Temperature Field Theory* (Cambridge University Press, Cambridge, England, 1989).

[42] W. M. Yao *et al.* (Particle Data Group), J. Phys. G **33**, 1 (2006).

[43] I. Caprini, G. Colangelo, and H. Leutwyler, Phys. Rev. Lett. **96**, 132001 (2006).

[44] J. Schaffner-Bielich, Phys. Rev. Lett. **84**, 3261 (2000).

[45] P. Costa, M. C. Ruivo, C. A. de Sousa, and Y. L. Kalinovsky, Phys. Rev. D **71**, 116002 (2005).

[46] T. Kunihiro, Phys. Lett. B **219**, 363 (1989); R. Alkofer, P. A. Amundsen, and H. Reinhardt, Phys. Lett. B **218**, 75 (1989).

[47] D. Horvatic, D. Klabucar, and A. E. Radzhabov, Phys. Rev. D **76**, 096009 (2007).

[48] D. Klabucar and D. Kekez, Phys. Rev. D **58**, 096003 (1998); D. Kekez and D. Klabucar, Phys. Rev. D **73**, 036002 (2006); D. Klabucar, D. Kekez, and M. D. Scadron, J. Phys. G **27**, 1775 (2001).

[49] F. Karsch, E. Laermann, and A. Peikert, Nucl. Phys. **B605**, 579 (2001).

[50] Y. Aoki, G. Endrodi, Z. Fodor, S. D. Katz, and K. K. Szabo, Nature (London) **443**, 675 (2006).

[51] P. Costa, M. C. Ruivo, and C. A. de Sousa, Phys. Rev. D **77**, 096001 (2008).

[52] S. Strueber and D. H. Rischke, Phys. Rev. D **77**, 085004 (2008).

[53] R. D. Pisarski and F. Wilczek, Phys. Rev. D **29**, 338 (1984).

[54] J. T. Lenaghan, Phys. Rev. D **63**, 037901 (2001).

[55] B.-J. Schaefer and M. Wagner (work in progress).